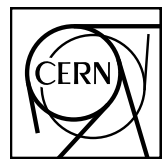


# EUROPEAN ORGANIZATION FOR NUCLEAR RESEARCH



ALICE-ANA-2022-xxx  
November 8, 2022

## D<sup>\*+</sup>-meson production in pp collisions at $\sqrt{s} = 13$ TeV

Syaefudin Jaelani<sup>1</sup>

1. Indonesian Institute of Sciences

Email: syaefudin.jaelani@cern.ch

### Abstract

The production of prompt D<sup>\*+</sup> meson and their anti-particles was measured using 2016, 2017, and 2018 data samples in pp collisions at  $\sqrt{s} = 13$  TeV. The production cross-section is measured at mid-rapidity as a function of  $p_T$ . The D<sup>\*+</sup> meson is reconstructed in the range  $1 < p_T < 50$  GeV/ $c$ .



## Contents

<b>1</b>	<b>Introduction</b>	<b>3</b>
1.1	Data sample . . . . .	3
1.2	Monte Carlo sample . . . . .	7
1.3	Code used for the analysis . . . . .	7
<b>2</b>	<b>D meson selection</b>	<b>8</b>
2.1	Single track selections . . . . .	8
2.2	Topological and kinematic selections . . . . .	8
2.3	Particle identification . . . . .	8
2.4	Signal extraction . . . . .	9
<b>3</b>	<b>Corrections</b>	<b>9</b>
<b>4</b>	<b>Systematic uncertainties</b>	<b>13</b>
4.1	Raw yield extraction . . . . .	13
4.2	Selection efficiency . . . . .	26
4.3	Generated $p_T$ shape . . . . .	29
4.4	PID efficiency . . . . .	32
4.5	Track reconstruction efficiency . . . . .	34
<b>5</b>	<b>Feed-down subtraction</b>	<b>34</b>
<b>6</b>	<b>Results</b>	<b>36</b>



## 1 Introduction

### 1.1 Data sample

The analyses note will discuss the production cross-section of D<sup>\*+</sup> meson in pp collisions at  $\sqrt{s} = 13$  TeV. The data samples used for this analysis are pp data at  $\sqrt{s} = 13$  TeV combined 2016, 2017, and 2018. The minimum bias triggered data of data samples, LHC2016\_deghjop, LHC2016\_kl, LHC2017\_cefhijklmor, and LHC2018\_bdefghijklmnop are used for this analysis. The run list used for this analysis, as selected after quality assurance checks, is as follows:

- **LHC2016\_AOD234\_deghjop\_13TeV**

**child 1:** 252375, 252374, 252371, 252370, 252368, 252336, 252332, 252330, 252326, 252325, 252322, 252319, 252317, 252310, 252271, 252248, 252235  
**child 2:** 253591, 253589, 253563, 253530, 253529, 253517, 253488, 253482, 253481, 253478, 253437, 252867, 252858  
**child 3:** 254332, 254331, 254330, 254304, 254303, 254302, 254293, 254205, 254204, 254199, 254193, 254178, 254175, 254174, 254149, 254147, 254128  
**child 4:** 255469, 255467, 255466, 255465, 255463, 255447, 255442, 255440, 255421, 255420, 255419, 255418, 255415, 255407, 255402, 255398, 255352, 255351, 255350, 255283, 255280, 255276, 255275, 255256, 255255, 255253, 255252, 255251, 255249, 255248, 255247, 255242, 255240, 255182, 255181, 255180, 255177, 255176, 255174, 255173, 255171, 255167, 255162, 255159, 255154, 255111, 255091, 255086, 255085, 255082, 255079, 254984, 254983, 254654, 254653, 254652, 254651, 254649, 254648, 254646, 254644, 254640, 254632, 254630, 254629, 254621, 254606, 254604, 254422, 254419, 254418  
**child 5:** 256418, 256417, 256415, 256373, 256372, 256371, 256368, 256366, 256365, 256364, 256363, 256362, 256361, 256356, 256311, 256309, 256307, 256302, 256299, 256297, 256295, 256292, 256290, 256289, 256287, 256284, 256283, 256282, 256281, 256231, 256228, 256227, 256225, 256223, 256219  
**child 6:** 264035, 264033, 263985, 263984, 263981, 263978, 263977, 263923, 263920, 263917, 263916, 263905, 263866, 263863, 263810, 263803, 263793, 263792, 263790, 263787, 263786, 263785, 263784, 263744, 263743, 263741, 263739, 263738, 263737, 263691, 263690, 263682, 263663, 263662, 263657, 263654, 263652, 263647, 263529, 263497, 263496, 263490, 263487, 263332, 263331, 262858, 262855, 262853, 262849, 262847, 262844, 262842, 262841, 262778, 262777, 262776, 262768, 262760, 262727, 262725, 262723, 262719, 262717, 262713, 262708, 262706, 262705, 262428, 262426, 262425, 262424, 263979, 262635, 262632, 262628, 262624, 262594, 262593, 262583, 262578, 262574, 262572, 262571, 262570, 262569, 262568, 262567, 262563, 262537, 262533, 262532, 262528, 262492, 262490, 262489, 262487, 262451, 262450, 262430, 263861  
**child 7:** 264347, 264346, 264345, 264341, 264336, 264312, 264306, 264305, 264281, 264279, 264277, 264273, 264267, 264266, 264265, 264264, 264262, 264261, 264260, 264259, 264238, 264235, 264233, 264232, 264198, 264197, 264194, 264190, 264188, 264168, 264164, 264139, 264138, 264137, 264129, 264110, 264109, 264086, 264085, 264082, 264078, 264076

- **LHC2016\_AOD234\_kl\_13TeV**

**child 1:** 258537, 258499, 258477, 258456, 258454, 258452, 258426, 258393, 258391, 258387, 258359, 258336, 258332, 258307, 258306, 258303, 258302, 258301, 258299, 258278, 258274, 258273, 258271, 258270, 258258, 258257, 258256, 258204, 258203, 258202, 258198, 258197, 258178, 258117, 258114, 258113, 258109, 258108, 258107, 258063, 258062, 258060, 258059, 258053, 258049, 258045, 258042, 258041, 258039, 258019, 258017, 258014, 258012, 258008, 258003, 257992, 257989, 257986, 257979, 257963, 257960, 257957, 257939, 257937, 257936,

257855, 257853, 257851, 257850, 257804, 257803, 257800, 257799, 257798, 257797, 257773, 257765, 257757, 257754, 257737, 257735, 257734, 257733, 257727, 257725, 257724, 257697, 257694, 257692, 257691, 257689, 257688, 257687, 257685, 257684, 257682, 257644, 257642, 257636, 257635, 257632, 257630, 257606, 257605, 257604, 257601, 257595, 257594, 257592, 257590, 257588, 257587, 257566, 257562, 257561, 257560, 257541, 257540, 257539, 257537, 257531, 257530, 257492, 257491, 257490, 257488, 257487, 257474, 257468, 257457, 257433, 257364, 257358, 257330, 257322, 257320, 257318, 257260, 257224, 257209, 257206, 257204, 257144, 257141, 257139, 257138, 257137, 257136, 257100, 257095, 257092, 257086, 257084, 257082, 257080, 257077, 257012, 257011, 256944, 256942, 256941, 258498, 258388, 258280, 257932, 257912, 257901, 257071

**child 2:** 259888, 259868, 259867, 259866, 259860, 259842, 259841, 259822, 259789, 259788, 259781, 259756, 259752, 259751, 259750, 259748, 259747, 259477, 259473, 259396, 259395, 259394, 259389, 259388, 259382, 259378, 259342, 259341, 259340, 259339, 259336, 259334, 259307, 259305, 259303, 259302, 259274, 259273, 259272, 259271, 259270, 259269, 259264, 259263, 259261, 259257, 259204, 259164, 259162, 259118, 259117, 259099, 259096, 259091, 259090, 259088, 258964, 258962, 259381, 259086

#### - LHC2017\_AOD234\_cefhijklmor\_13TeV\_pp

**child 1:** 270830, 270828, 270827, 270824, 270822

**child 2:** 270865, 270861, 270856, 270855, 270854

**child 3:** 273103, 273100, 273099, 273077, 273010, 273009, 272985, 272983, 272976, 272949, 272947, 272939, 272935, 272934, 272933, 272932, 272905, 272903, 272880, 272873, 272871, 272870, 272836, 272834, 272833, 272829, 272828, 272784, 272783, 272782, 272764, 272763, 272760, 272749, 272747, 272712, 272691, 272690, 272620, 272610, 272608, 272607, 272585, 272577, 272575, 272574, 272521, 272468, 272466, 272463, 272462, 272461, 272413, 272411, 272400, 272399, 272395, 272394, 272389, 272388, 272360, 272359, 272340, 272335, 272194, 272156, 272155, 272154, 272153, 272152, 272151, 272123, 272101, 272100, 272076, 272042, 272040, 272039, 272038, 272036, 272020, 272018, 271886, 271880, 271874, 271873, 271871, 271870, 273101, 272762, 272469, 272417, 272414, 272075

**child 4:** 274442, 274390, 274389, 274388, 274387, 274386, 274385, 274364, 274363, 274360, 274352, 274329, 274283, 274281, 274280, 274278, 274276, 274271, 274270, 274269, 274268, 274266, 274264, 274263, 274259, 274258, 274232, 274212, 274174, 274148, 274147, 274125, 274094, 274092, 274058, 273986, 273985, 273946, 273943, 273942, 273918, 273889, 273887, 273886, 273885, 273825, 273824, 273654, 273653, 273593, 273592, 273591, 274357, 274355, 274063

**child 5:** 274671, 274669, 274667, 274657, 274653, 274601, 274596, 274595, 274594, 274593

**child 6:** 276508, 276507, 276506, 276462, 276439, 276438, 276437, 276435, 276351, 276348, 276302, 276297, 276294, 276292, 276290, 276259, 276257, 276230, 276205, 276178, 276177, 276170, 276169, 276166, 276145, 276140, 276135, 276104, 276102, 276099, 276098, 276097, 275847, 275664, 275661, 275650, 275648, 275647, 275624, 275623, 275622, 275621, 275617, 275612, 275559, 275558, 275515, 275472, 275471, 275467, 275459, 275457, 275456, 275453, 275452, 275448, 275443, 275406, 275404, 275401, 275372, 275369, 275361, 275360, 275333, 275332, 275328, 275326, 275324, 275322, 275314, 275283, 275247, 275246, 275245, 275239, 275188, 275184, 275180, 275177, 275174, 275173, 275151, 275150, 275149, 275076, 275075, 275073, 275068, 275067, 274979, 274978, 274886, 274882, 274878, 274877, 274822, 274821, 274815, 274806, 274803, 274802, 274801, 274708, 274690, 274736, 274883, 274884, 274889, 276105, 276108, 276141

**child 7:** 278216, 278215, 278191, 278189, 278167, 278166, 278165, 278164, 278158, 278127, 278126, 278123, 278122, 278121, 277996, 277991, 277989, 277987, 277952, 277930, 277907, 277904, 277903, 277900, 277899, 277898, 277897, 277876, 277870, 277848, 277847, 277845,

277842, 277841, 277836, 277834, 277805, 277802, 277801, 277800, 277799, 277795, 277794, 277749, 277747, 277746, 277745, 277725, 277723, 277722, 277721, 277577, 277576, 277575, 277574, 277537, 277536, 277534, 277531, 277530, 277479, 277478, 277477, 277476, 277473, 277472, 277418, 277417, 277416, 277389, 277386, 277385, 277384, 277383, 277360, 277314, 277312, 277310, 277293, 277262, 277257, 277256, 277197, 277196, 277194, 277193, 277189, 277188, 277184, 277183, 277182, 277181, 277180, 277155, 277121, 277117, 277091, 277087, 277082, 277079, 277076, 277073, 277037, 277017, 277016, 277015, 276972, 276971, 276970, 276969, 276967, 276920, 276917, 276916, 276762, 276675, 276674, 276672, 276671, 276670, 276644, 276608, 276557, 276556, 276553, 276552, 276551, 278130, 277988, 277470, 276669  
**child 8:** 280140, 280135, 280134, 280131, 280126, 280118, 280114, 280111, 280108, 280107, 280066, 280052, 280051, 279879, 279855, 279854, 279853, 279830, 279827, 279826, 279773, 279749, 279747, 279719, 279718, 279715, 279689, 279688, 279687, 279684, 279683, 279682, 279679, 279677, 279676, 279642, 279641, 279632, 279630, 279559, 279550, 279491, 279488, 279487, 279483, 279441, 279439, 279435, 279410, 279391, 279355, 279354, 279349, 279348, 279344, 279342, 279312, 279310, 279309, 279274, 279273, 279270, 279268, 279267, 279265, 279264, 279242, 279238, 279235, 279234, 279232, 279208, 279207, 279201, 279199, 279157, 279155, 279130, 279123, 279122, 279118, 279117, 279107, 279106, 279075, 279074, 279073, 279069, 279068, 279044, 279043, 279041, 279036, 279035, 279008, 279007, 279005, 279000, 278999, 278964, 278963, 278960, 278959, 278941, 278939, 278936, 278915, 278914  
**child 9:** 282704, 282703, 282702, 282700, 282677, 282676, 282673, 282671, 282670, 282667, 282666, 282651, 282629, 282622, 282620, 282618, 282609, 282608, 282607, 282606, 282580, 282579, 282575, 282573, 282546, 282545, 282544, 282528  
**child 10:** 280283, 280284, 280285, 280286, 280290, 280310, 280312, 280348, 280349, 280350, 280351, 280374, 280375, 280403, 280405, 280406, 281961, 281956, 281953, 281940, 281939, 281932, 281931, 281928, 281920, 281918, 281916, 281915, 281895, 281894, 281893, 281892, 281633, 281592, 281583, 281574, 281569, 281568, 281563, 281562, 281557, 281511, 281509, 281477, 281475, 281450, 281449, 281446, 281444, 281443, 281441, 281415, 281321, 281301, 281277, 281275, 281273, 281271, 281244, 281243, 281242, 281241, 281240, 281213, 281212, 281191, 281190, 281189, 281181, 281180, 281179, 281081, 281080, 281062, 281061, 281060, 281036, 281035, 281033, 281032, 280999, 280998, 280997, 280996, 280994, 280990, 280947, 280943, 280940, 280936, 280897, 280880, 280856, 280854, 280849, 280848, 280847, 280844, 280842, 280793, 280792, 280787, 280786, 280768, 280767, 280766, 280765, 280764, 280763, 280762, 280761, 280757, 280756, 280755, 280754, 280753, 280729, 280706, 280705, 280681, 280679, 280671, 280647, 280645, 280639, 280637, 280636, 280634, 280613, 280583, 280581, 280574, 280551, 280550, 280547, 280546, 280519, 280518, 280499, 280490, 280448, 280447, 280446, 280445, 280443, 280419, 280415, 280412, 281756, 281755, 281754, 281753, 281751, 281750, 281741, 281713, 281709, 281707, 281706, 281705, 281581, 281580, 280676, 280673, 280650, 280648, 280352

#### – LHC2018\_AOD264\_bdefghijklmnop\_13TeV

**child 1:** 286350, 286349, 286348, 286345, 286341, 286340, 286337, 286336, 286314, 286313, 286312, 286311, 286310, 286309, 286308, 286289, 286288, 286287, 286284, 286282, 286263, 286261, 286258, 286257, 286254, 286231, 286230, 286229, 286203, 286202, 286201, 286199, 286198, 286159, 286130, 286129, 286127, 286124, 286064, 286025, 286027, 286014, 285980, 285979, 285978, 286028, 286030

**child 2:** 286937, 286936, 286933, 286932, 286931, 286930, 286911, 286910, 286907, 286877, 286876, 286874, 286852, 286850, 286846, 286809, 286805, 286801, 286799, 286731, 286695, 286661, 286653, 286633, 286592, 286591, 286569, 286568, 286567, 286566, 286511, 286509, 286508, 286502, 286482, 286455, 286454, 286428, 286427, 286426, 286380

**child 3:** 287658, 287657, 287656, 287654, 287578, 287575, 287524, 287521, 287518, 287517,

287516, 287513, 287486, 287484, 287481, 287480, 287451, 287413, 287389, 287388, 287387, 287385, 287381, 287380, 287360, 287356, 287355, 287353, 287349, 287347, 287346, 287344, 287343, 287325, 287324, 287323, 287283, 287254, 287251, 287250, 287249, 287248, 287209, 287208, 287204, 287203, 287202, 287201, 287185, 287155, 287137, 287077, 287072, 287071, 287066, 287064, 287063, 287021, 287000, 287977, 287975, 287941, 287923, 287915, 287913, 287912, 287911, 287885, 287884, 287877, 287876, 287784, 287783

**child 4:** 288619, 288640, 288642, 288644, 288650, 288687, 288689, 288690, 288743, 288748, 288750

**child 5:** 288804, 288806

**child 6:** 288861, 288862, 288863, 288864, 288868, 288902, 288903, 288908, 288909, 288897

**child 7:** 288943

**child 8:** 289165, 289166, 289167, 289169, 289172, 289175, 289176, 289177, 289198, 289199, 289200, 289201

**child 9:** 289971, 289966, 289965, 289943, 289941, 289940, 289935, 289931, 289928, 289884, 289880, 289879, 289857, 289856, 289855, 289854, 289852, 289849, 289830, 289818, 289817, 289816, 289815, 289814, 289811, 289808, 289775, 289757, 289732, 289731, 289729, 289724, 289723, 289721, 289666, 289664, 289660, 289659, 289658, 289657, 289634, 289632, 289625, 289582, 289577, 289576, 289574, 289547, 289521, 289494, 289493, 289468, 289466, 289465, 289463, 289462, 289444, 289426, 289374, 289373, 289370, 289369, 289368, 289367, 289366, 289365, 289356, 289355, 289354, 289353, 289309, 289308, 289306, 289303, 289300, 289281, 289280, 289278, 289277, 289276, 289275, 289254, 289253, 289249, 289247, 289243, 289242, 289241, 289240, 289666, 289664, 289660, 289659, 289658, 289657, 289634, 289632, 289625, 289582, 289577, 289576, 289574

**child 10:** 292839, 292836, 292834, 292832, 292831, 292811, 292810, 292809, 292804, 292803, 292752, 292750, 292748, 292747, 292744, 292739, 292737, 292704, 292701, 292698, 292696, 292695, 292693, 292586, 292584, 292563, 292560, 292559, 292557, 292554, 292553, 292526, 292524, 292523, 292521, 292500, 292497, 292496, 292495, 292461, 292460, 292457, 292456, 292434, 292432, 292430, 292429, 292428, 292406, 292405, 292398, 292397, 292298, 292273, 292265, 292242, 292241, 292240, 292218, 292192, 292168, 292167, 292166, 292164, 292163, 292162, 292161, 292160, 292140, 292115, 292114, 292109, 292108, 292107, 292106, 292081, 292080, 292077, 292075, 292067, 292062, 292061, 292060, 292040, 292012, 291982, 291977, 291976, 291953, 291948, 291946, 291945, 291944, 291943, 291942, 291803, 291796, 291795, 291769, 291768, 291766, 291762, 291760, 291756, 291755, 291729, 291706, 291698, 291697, 291690, 291665, 291661, 291657, 291626, 291624, 291622, 291618, 291615, 291614, 291590, 291485, 291484, 291482, 291481, 291457, 291456, 291453, 291451, 291447, 291424, 291420, 291417, 291416, 291402, 291400, 291399, 291397, 291377, 291375, 291373, 291363, 291362, 291361, 291360, 291286, 291285, 291284, 291282, 291266, 291265, 291263, 291262, 291257, 291240, 291209, 291188, 291143, 291116, 291111, 291110, 291101, 291100, 291093, 291069, 291066, 291065, 291041, 291037, 291035, 291006, 291005, 291004, 291003, 291002, 290980, 290979, 290976, 290975, 290974, 290948, 290944, 290943, 290941, 290935, 290932, 290895, 290894, 290888, 290887, 290886, 290862, 290860, 290853, 290848, 290846, 290843, 290841, 290790, 290787, 290766, 290689, 290687, 290665, 290660, 290645, 290632, 290627, 290615, 290614, 290613, 290612, 290590, 290588, 290553, 290550, 290549, 290544, 290540, 290539, 290538, 290501, 290500, 290499, 290469, 290467, 290459, 290458, 290456, 290427, 290426, 290425, 290423, 290412, 290411, 290404, 290401, 290399, 290376, 290375, 290374, 290350, 290327, 290323, 291373

**child 11:** 293357, 293359

**child 12:** 293898, 293896, 293893, 293891, 293886, 293856, 293831, 293830, 293829, 293809, 293807, 293806, 293805, 293802, 293776, 293774, 293773, 293770, 293741, 293740, 293698, 293696, 293695, 293692, 293691, 293588, 293587, 293583, 293582, 293579, 293578, 293573,

293571, 293570, 293475, 293496, 293494, 293474, 293424, 293413, 293392, 293386, 293368  
**child 13:** 294925, 294916, 294884, 294883, 294880, 294875, 294852, 294818, 294817, 294816,  
294815, 294813, 294809, 294805, 294775, 294774, 294772, 294769, 294749, 294747, 294746,  
294745, 294744, 294742, 294741, 294722, 294718, 294715, 294710, 294703, 294653, 294636,  
294633, 294632, 294593, 294591, 294590, 294587, 294586, 294563, 294562, 294558, 294556,  
294553, 294531, 294530, 294529, 294527, 294526, 294525, 294524, 294310, 294308, 294307,  
294305, 294242, 294241, 294212, 294210, 294208, 294205, 294201, 294200, 294199, 294156,  
294155, 294154, 294152, 294131, 294013, 294012, 294011, 294010, 294009  
**child 14:** 285396, 285365, 285364, 285347, 285328, 285327, 285224, 285222, 285203, 285202,  
285200, 285165, 285127, 285125, 285108, 285106, 285066, 285065, 285064, 285015, 285014,  
285013, 285012, 285011, 285009

## 1.2 Monte Carlo sample

The Monte-Carlo (MC) sample used for the corrections is anchored to the runlists reported above and generated with the same detector configurations as the data productions. In particular three production cycles are used LHC20f4a\_2018\_P8, LHC20f4b\_2017\_P8, and LHC20f4c\_2016\_P8. The Monte Carlo sample are generated with HIJING + HF Pythia8 events. Each pp event was required to contain at least one charm or beauty quark-antiquark pair. The following heavy-flavour hadrons are forced to decay via their hadronic decay channels. The run numbers used for the MC are the same as stated above for LHC2016, LHC2017, and LHC2018 samples.

## 1.3 Code used for the analysis

The results reported in this analysis note obtained with code available on AliPhysics Git master branch and more precisely in PWGHF/vertexingHF. The D<sup>\*+</sup> invariant mass distributions are obtained by using the task `AliAnalysisTaskSEDStarSpectra.cxx`. It reads the AOD event and looks over the D<sup>\*+</sup> candidates stored in the delta AOD, `AliAOD.VertexingHF`, at the filtering time. Single track, topological selections as well as particle identification are applied by using the class `AliRDHFDstartoKpipi` and the actual values of the cuts are read from a cut object saved as root file. The cut object is created using the AliRoot macro named `makeTFileDstartoKpipi`. The `AliHFInvMassFitter` was used to fit invariant mass distributions and estimate raw yields.

The D<sup>\*+</sup> meson cut objects is also provided to the `AliAnalysisTaskCFVertexingHF`, which is the task used for the efficiencies evaluation for the correction of the raw yields. The results presented in this note are obtained by using ALICE LEGO trains. The results reported here are extracted from the output of the D2H pp LEGO trains. In particular, the data train numbers 4371-4374 and MC train numbers 3855-3857 were used. The topological selections used for the analyses can be found later in this note and are even saved in the LEGO train output.

## 2 D meson selection

The  $D^{*+}$  meson and their anti-particles was reconstructed in the central rapidity region by exploiting their charged hadronic decay channels:  $D^{*+} \rightarrow D^0 \pi^+$  (with  $B.R. = 67.7 \pm 0.5\%$ ), while the  $D^0$  meson decay into  $K^-$  and  $\pi^+$  with branching ratio  $(3.93 \pm 0.04)\%$ . The  $D^{*+}$  decay proceeds via strong interaction, thus making impossible the secondary vertex reconstruction. The analysis exploits topological selections on the  $D^0$ , together with the sharp peak in the difference between the invariant mass of the three final state hadrons and that of the two  $D^0$  decay prongs. Since the mass difference  $\Delta m = m_{D^{*+}} - m_{D^0} \approx 145.4$  MeV/c is only slightly larger than the charged pion mass. For low  $p_T$   $D^{*+}$  mesons the produced pion has typically low momentum and is referred to here as a soft pion.

### 2.1 Single track selections

The  $D^{*+}$  candidates were formed by combining  $D^0$  candidates with soft pion  $\pi^+$  tracks having  $|\eta| < 0.8$  and  $p_T > 0.3$  GeV/c, also satisfying the kITSrefit and kTPCrefit conditions. Moreover, for all the tracks, a minimum number of 70 crossed rows in the TPC together with a crossed rows over findable clusters ratio of 0.8 was required, and  $\chi^2/ndf < 2$  in the TPC. A cut on the transverse impact parameter  $d_0$  was applied for tracks with  $p_T < 2$  GeV/c, requiring  $d_0 > 50 \mu\text{m}$ . These selections were meant to limit the CPU time needed to perform the track combinatorics when creating the AODs with the D meson candidates. Furthermore, the  $D^{*+}$  soft pions were selected requiring at least one associated hit in either of the two SPD layers.

### 2.2 Topological and kinematic selections

The  $D^{*+}$  signal extraction is based on topological selections of displaced secondary vertices from  $D^0$ -meson candidates. For a detailed explanation of the procedure refer to [1]. The topological and kinematic cuts used to select the  $D^{*+}$ -meson signal in pp collisions at  $\sqrt{s} = 13$  TeV are reported in Table 1 and 2.

**Table 1:** Selections used for the  $D^{*+}$ -meson in the transverse momentum intervals  $1 < p_T < 6.5$  GeV/c.

$p_T$ (GeV/c) variable	[1-1.5]	[1.5-2]	[2-2.5]	[2.5-3]	[3-3.5]	[3.5-4]	[4-4.5]	[4.5-5]	[5-5.5]	[5.5-6]	[6-6.5]
$\Delta M_{D^0}$ (GeV)	0.021	0.032	0.035	0.035	0.038	0.038	0.038	0.042	0.042	0.045	0.049
DCA (cm)	0.022	0.038	0.03	0.03	0.03	0.03	0.042	0.042	0.05	0.05	0.1
$\text{Cos}(\theta^*)$	0.9	0.9	0.8	0.8	0.8	0.8	0.9	0.9	1.0	1.0	1.0
$p_T(K)$ (GeV/c)	0.4	0.4	0.9	0.9	0.9	1.0	1.0	1.0	1.0	1.0	1.0
$p_T(\pi)$ (GeV/c)	0.4	0.4	0.9	0.9	0.9	1.0	1.0	1.0	1.0	1.0	1.0
$d_{0,K}$ (cm)	0.1	0.1	0.1	0.1	0.1	0.1	0.1	0.1	0.1	0.1	0.1
$d_{0,\pi}$ (cm)	0.1	0.1	0.1	0.1	0.1	0.1	0.1	0.1	0.1	0.1	0.1
$d_{0,K} \times d_{0,\pi} (10^{-3}) (\text{cm}^2)$	-0.00025	-0.00025	-0.00019	-0.00019	-0.000144	-0.000144	$-2.8 \times 10^{-5}$	$-2.8 \times 10^{-5}$	$5.5 \times 10^{-5}$	$5.5 \times 10^{-5}$	0.0001
$\text{Cos}(\theta_{point})$	0.8	0.8	0.9	0.9	0.89	0.89	0.81	0.81	0.79	0.79	0.7
Inv. mass half width of $D^{*+}$ (GeV)	0.3	0.3	0.3	0.3	0.3	0.3	0.3	0.3	0.3	0.3	0.3
hal width of $\Delta M$ (GeV)	0.3	0.3	0.3	0.3	0.3	0.3	0.3	0.3	0.3	0.3	0.3
$p_T$ soft $\pi$ min (GeV/c)	0.05	0.05	0.05	0.05	0.05	0.05	0.05	0.05	0.05	0.05	0.05
$p_T$ soft $\pi$ max (GeV/c)	0.3	0.3	0.4	0.4	0.6	0.6	0.6	100	100	100	100
$\theta$	1.0	1.0	1.0	1.0	1.0	1.0	1.0	1.0	1.0	1.0	1.0
$ \text{Cos}(\theta_{point})XY $	0.88	0.88	-1.	-1.	-1.	-1.	-1.	-1.	-1.	-1.	-1.
NL <sub>XY</sub>	3.	3.	3.	3.	0	0	0	0	0	0	0

### 2.3 Particle identification

The identification of the charged kaons and pions in the TPC and TOF detectors provide an additional information for the background rejection in the low momentum region. In order to assign K and/or  $\pi$  masses to the decay tracks, cuts are applied to the difference in the expected and measured signals, which are the specific energy deposited ( $dE/dx$ ) in the TPC and the time-of-flight for the TOF. A  $3\sigma$  compatibility was required to  $D^{*+}$  candidate's daughters. When tracks were without TOF signal, only the TPC particle identification was used. Tracks with contradicting particle identification were considered to be non-identified and retained for further analysis.

**Table 2:** Selections used for the D<sup>\*+</sup>-meson in the transverse momentum intervals  $6.5 < p_T < 50$  GeV/ $c$ .

$p_T$ (GeV/ $c$ ) variable	[6.5-7]	[7-7.5]	[7.5-8]	[8-9]	[9-10]	[10-12]	[12-16]	[16-24]	[24-36]	[36-50]
$\Delta M_{D^0}$ (GeV)	0.049	0.052	0.052	0.056	0.056	0.074	0.074	0.074	0.074	0.074
DCA (cm)	0.1	0.1	0.1	0.1	0.1	0.1	0.1	0.1	10	10
$\text{Cos}(\theta^*)$	1.0	1.0	1.0	1.0	1.0	1.0	1.0	1.0	10	10
$p_T(K)$ (GeV/ $c$ )	1.0	0.6	0.6	0.6	0.6	0.6	0.6	0.5	0.2	0.2
$p_T(\pi)$ (GeV/ $c$ )	1.0	0.6	0.6	0.6	0.6	0.6	0.6	0.5	0.2	0.2
$d_{0,K}$ (cm)	0.1	0.1	0.1	0.1	0.1	0.1	0.1	0.15	0.5	0.5
$d_{0,\pi}$ (cm)	0.1	0.1	0.1	0.1	0.1	0.1	0.1	0.15	0.5	0.5
$d_{0,K} \times d_{0,\pi} (10^{-3})$ (cm <sup>2</sup> )	0.0001	0.0001	0.00019	0.0001	0.0001	0.001	0.001	1.	1.	1.
$\text{Cos}(\theta_{point})$	0.7	0.7	0.7	0.7	0.7	0.7	0.7	0.2	0.2	0.2
Inv. mass half width of D <sup>*+</sup> (GeV)	0.3	0.3	0.3	0.3	0.3	0.3	0.3	0.3	0.3	0.3
hal width of $\Delta M$ (GeV)	0.3	0.3	0.3	0.3	0.3	0.3	0.3	0.3	0.3	0.3
$p_T$ soft $\pi$ min (GeV/ $c$ )	0.05	0.05	0.05	0.05	0.05	0.05	0.05	0.05	0.05	0.05
$p_T$ soft $\pi$ max (GeV/ $c$ )	100	100	100	100	100	100	100	100	100	100
$\theta$	1.0	1.0	1.0	1.0	1.0	1.0	1.0	1.0	1.0	1.0
$ \text{Cos}(\theta_{point})XY $	-1.	-1.	-1.	-1.	-1.	-1.	-1.	-1.	-1.	-1.
NL <sub>XY</sub>	0	0	0	0	0	0	0	0	0	0

## 2.4 Signal extraction

The D<sup>\*+</sup> raw yields were extracted by performing a fit to the mass difference  $\Delta M = M(K\pi\pi) - M(K\pi)$  distributions and the term describing the background shape is an exponential convoluted with a power law according to the equation:

$$f_{bkg} = a \sqrt{\Delta M - m_\pi} \cdot e^{b(\Delta M - m_\pi)} \quad (1)$$

where  $m_\pi$  is the pion mass and  $a$  and  $b$  are free parameters.

The D<sup>\*+</sup>  $\Delta M$  invariant mass distribution is shown in Figure 1. For  $p_T$  1-1.5 GeV/ $c$ , the Power function was used to described the background shape. Figures 4 show that the Power function was better to describe the background shape than the function mentioned above, Power Law  $\times$  Exponential function. The D<sup>\*+</sup> signal was successfully extracted in the range  $1 < p_T < 50$  GeV/ $c$ . The goodness of the mass fit against the Monte Carlo (MC) expectations was checked in terms of mass peak  $\sigma$  and position. The comparisons of the Gaussian width and mean of the D<sup>\*+</sup> meson mass peaks in data and MC are reported in figure 2.

## 3 Corrections

The raw yields extracted from the fits to the invariant-mass distributions of D-meson candidates were corrected to obtain the pT -differential production cross sections of prompt (i.e. not coming from weak decays of B mesons) D mesons. For example, in the case of D<sup>\*+</sup> mesons, the production cross section was calculated as:

$$\frac{d\sigma^{D^{*+}}}{dp_T} \Big|_{|y|<0.5} = \frac{1}{\Delta p_T} \frac{1}{BR \cdot L_{int}} \frac{f_{\text{prompt}}(p_T) \cdot \frac{1}{2} N^{D^{*+}\text{raw}}(p_T)}{2y_{\text{fid}}(p_T)(\text{Acc} \times \varepsilon)_{\text{prompt}}(p_T)} \quad (2)$$

where  $N^{D^{*+}\text{raw}}$  ( $p_T$ ) are the values of the raw yields (sum of particles and antiparticles), which were corrected for the B-meson decay feed-down contribution (i.e. multiplied by the prompt fraction  $f_{\text{prompt}}$ ), divided by the acceptance-times-efficiency for prompt D<sup>\*+</sup> mesons,  $(\text{Acc} \times \varepsilon)_{\text{prompt}}$ , and divided by a factor of two to obtain the charge (particle and antiparticle) averaged yields. The corrected yields were divided by the decay channel branching ratio (BR), the pT interval width ( $\Delta p_T$ ), the rapidity coverage ( $2y_{\text{fid}}$ ) and the integrated luminosity  $L_{int}$ . The integrated luminosity as computed from the number of

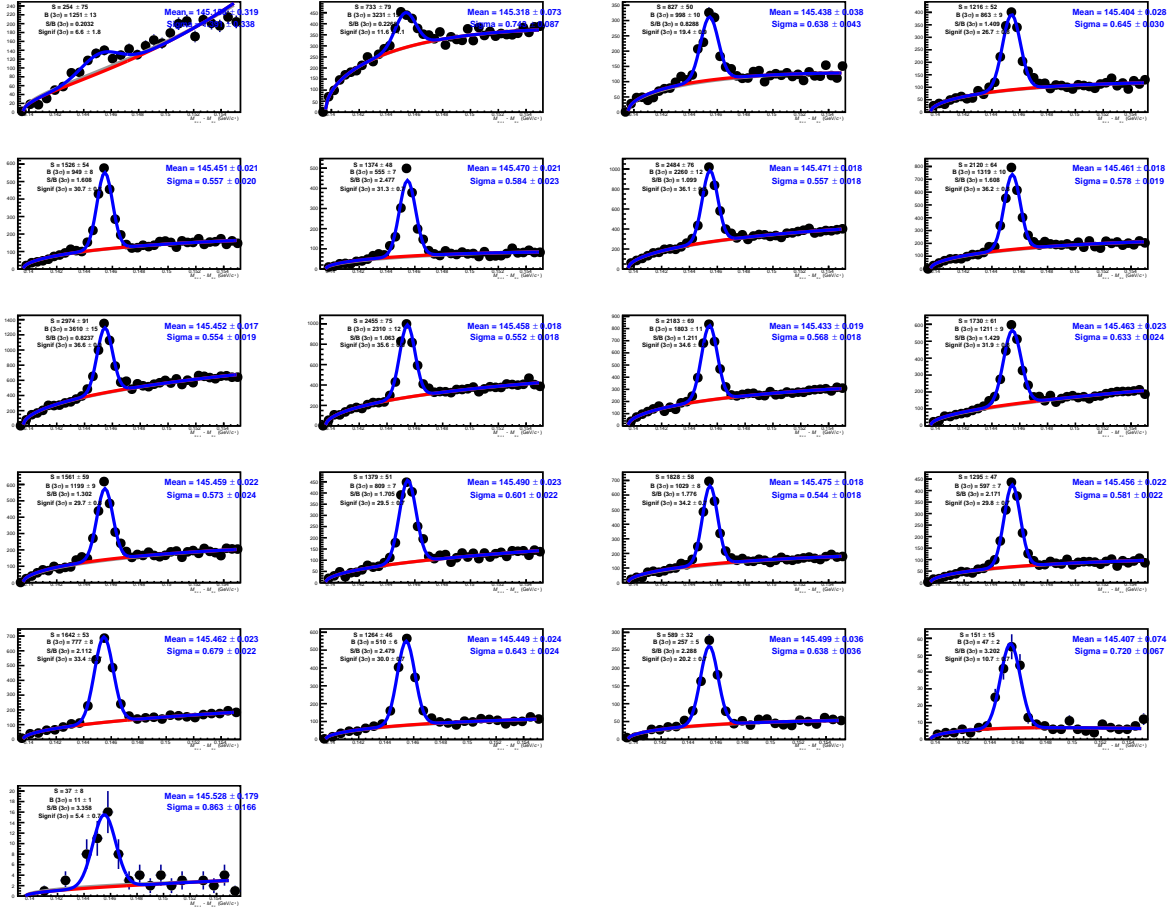


**Fig. 1:** Invariant mass distributions of ( $D^{*+} - D^0$ ) candidates and charge conjugates in the range  $1 < p_T < 50$  GeV/c.

analyzed events and the cross section of pp collisions passing the minimum-bias trigger condition,  $\sigma_{pp}$ , MB = 57.95 mb, derived from a van der Meer scan measurement.

The acceptance and efficiency correction factors, ( $\text{Acc} \times \varepsilon$ ), were determined using Monte Carlo simulations of pp collisions generated with the PYTHIA8 event generator with the Perugia-0 tune. The particles were propagated through the apparatus using both the GEANT transport codes. The luminous region distribution and the conditions (active channels, gain, noise level, and alignment) of all the ALICE detectors were included in the simulations, considering also their evolution with time during the LHC data taking period. The MC productions used to compute the ( $\text{Acc} \times \varepsilon$ ) only events containing a  $c\bar{c}$  or a  $b\bar{b}$  pair were transported through the apparatus and reconstructed. Moreover, D mesons were forced to decay in the hadronic channels considered in this analysis. The efficiency was extracted separately for prompt  $D^{*+}$  and  $D^{*+}$  coming from B-meson decays (feed-down). The results are reported in figure 5.

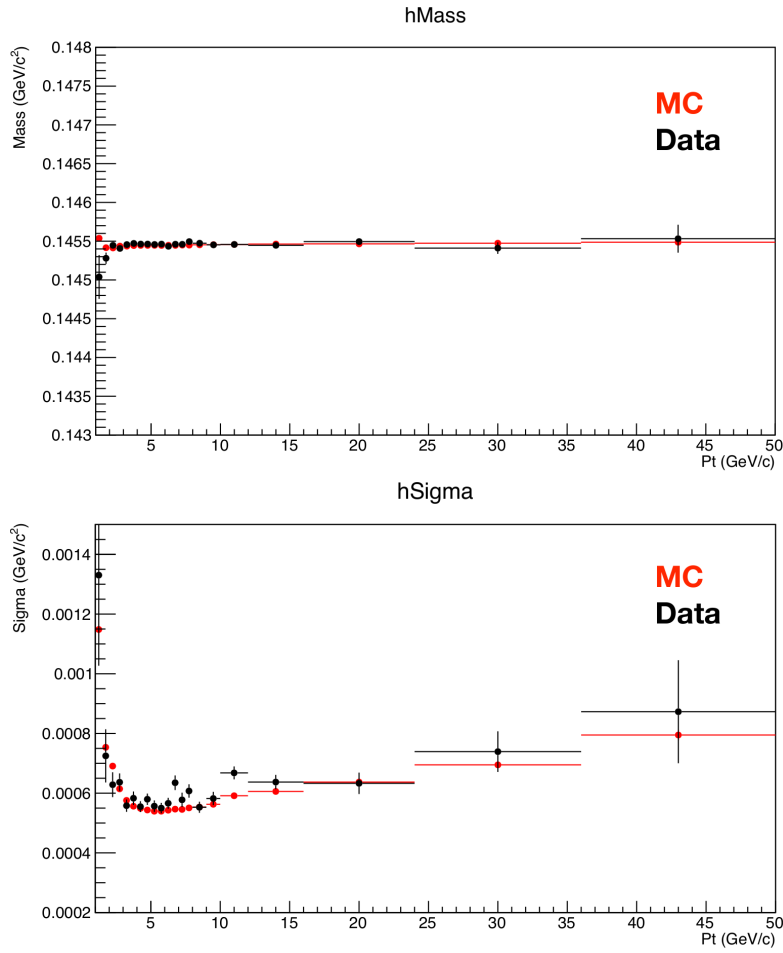


**Fig. 2:** Comparison of Gaussian mean (top) and width (bottom) extracted from the invariant-mass fits of D<sup>\*+</sup> candidates (black) and the MC simulation (red).

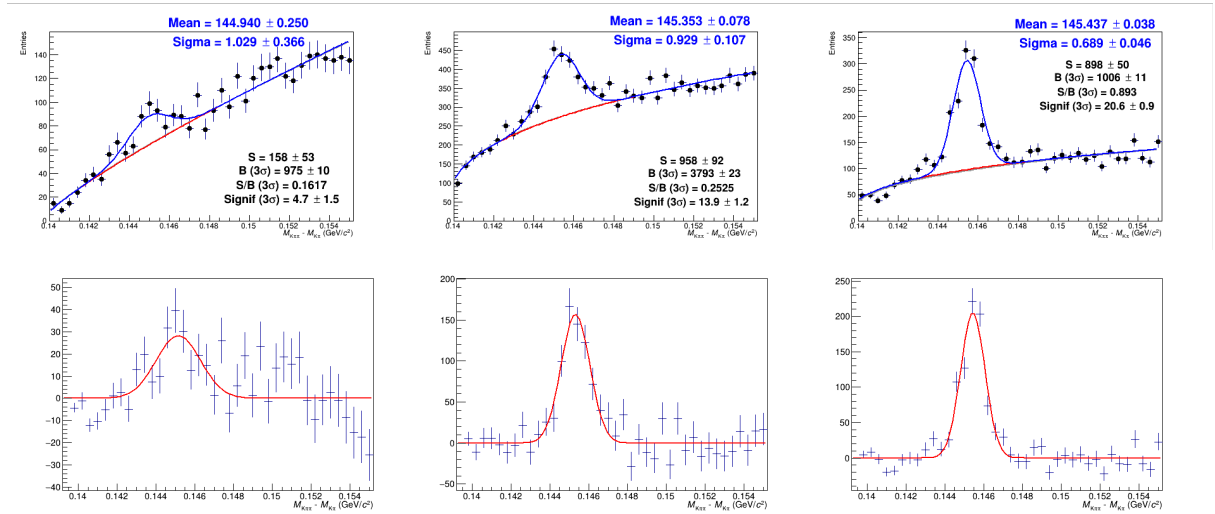


**Fig. 3:** The D<sup>\*+</sup>  $\Delta M$  invariant mass distribution for  $p_T$  range 1-2.5 GeV/c (top rows) with the Power  $\times$  Exponential function for describing the background shape and the residual plots (bottom rows).

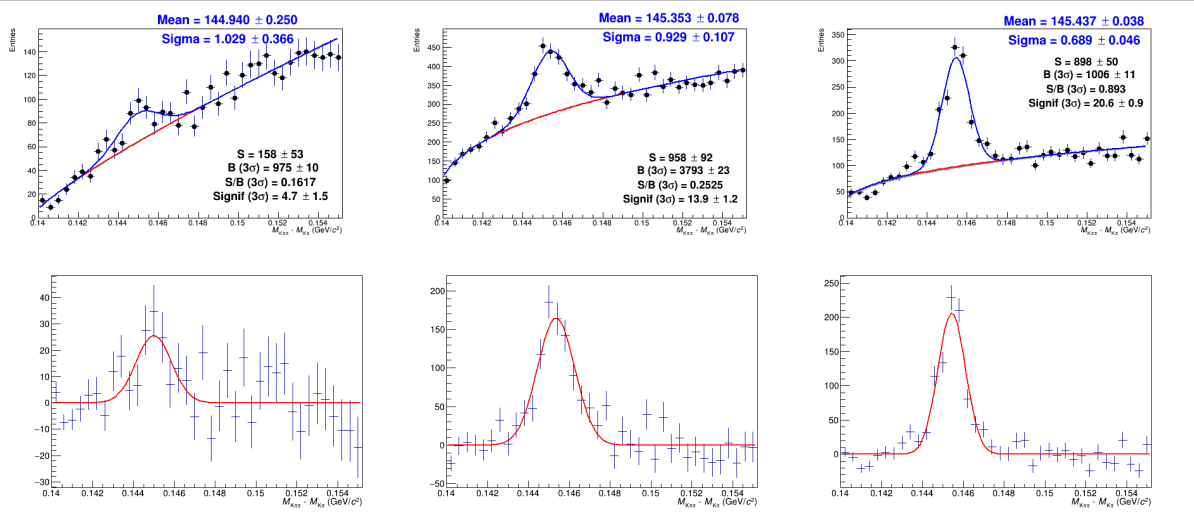


**Fig. 4:** The  $D^{*+}$   $\Delta M$  invariant mass distribution for  $p_T$  range 1-2.5 GeV/ $c$  (top rows) with the Power Law function for describing the background shape and the residual plots (bottom rows).

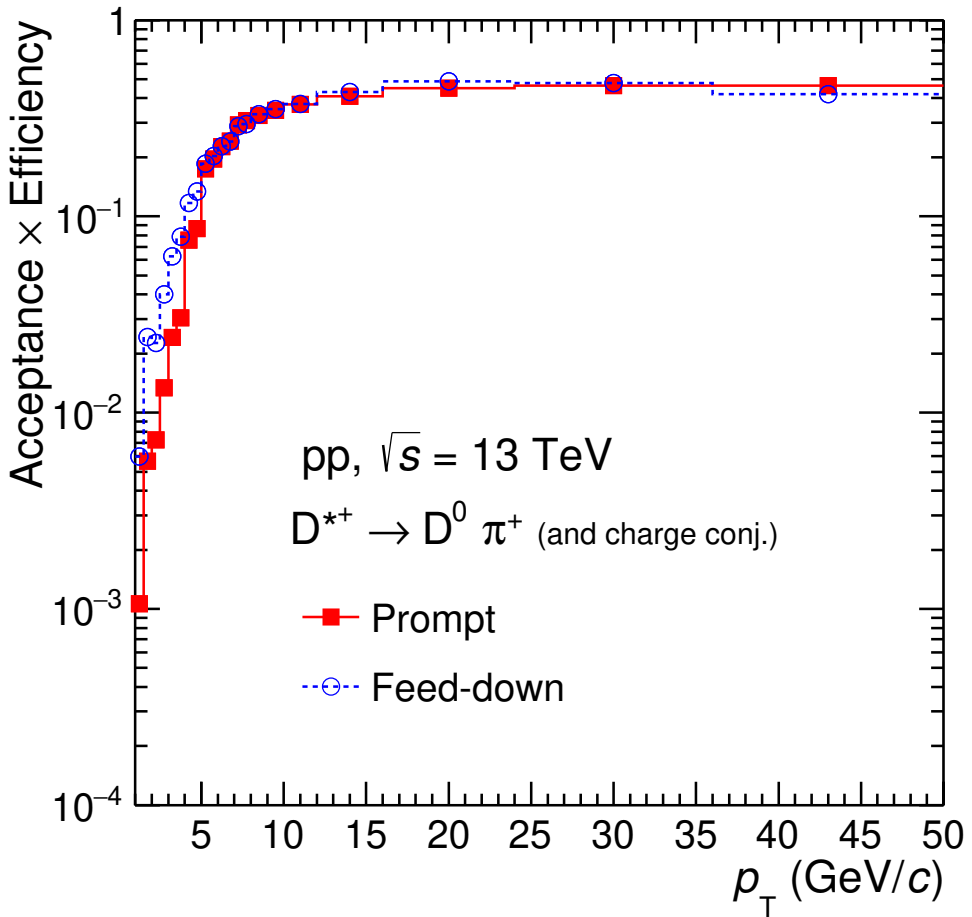


**Fig. 5:** Transverse momentum dependence of efficiency  $\times$  acceptance for prompt (black) and feed-down (red).

## 4 Systematic uncertainties

### 4.1 Raw yield extraction

Several sources of systematic errors were considered for the four D mesons. The systematic error on the yield extraction was determined by repeating the fitting procedure described in section 2.4 with a different mass range, different histogram bin widths and/or different fitting functions, and using a method based on bin counting after the subtraction of the background estimated from the fit of the side bands. For the D<sup>0</sup> meson, the variations listed above are obtained considering the yields once the reflection contribution has been subtracted.

The systematic uncertainty on the D<sup>+</sup>, D<sup>0</sup>, D<sup>\*+</sup> and D<sub>s</sub><sup>+</sup> raw yield extraction was evaluated in each  $p_T$  interval using a multiple trial approach. The fits to the invariant mass distributions were repeated several times varying:

- i) the invariant-mass bin width;
- ii) lower limit of the fit;
- iii) upper limit of the fit;
- iv) for D<sup>0</sup>, D<sup>+</sup>, and D<sub>s</sub><sup>+</sup>, the background fit function (3 cases: exponential, linear and second order polynomial);

In addition, all the fits were repeated with the sigma of the Gaussian function fixed to the values obtained from the MC simulation and the mean of the Gaussian function to the PDG value of the considered D-meson species mass. The fits which did not converge or had  $\chi^2/ndf > 2.0$  were rejected and not considered in the evaluation of the systematic uncertainty. In addition, the results obtained with the fitting technique were compared to those obtained by counting the entries in the invariant mass histogram after subtracting the background counts calculated from the background fit function. Also for this check, a multiple trial approach was used. The results for D<sup>+</sup> are shown in Figs. XX and YY, for the D<sup>0</sup> in Figs. XX and YY, for D<sup>\*+</sup> in Figs. XX and YY, and for D<sub>s</sub><sup>+</sup> in Figs. ??, ?? and YY. For the D<sup>0</sup> mesons the reflections subtraction procedure does not show a systematic effect, thus there is no need to assign a systematic uncertainty, as already shown in [2]. For the systematic uncertainty we took it almost from the rms of fit results. If the central raw yield between the mean of fit and bin counting doesn't differ, we do not consider the effect of shift; if not, we add in quadrature to the rms the maximum difference between the central value and the mean of the fits or of the bin counting.

The numerical values of the systematic on yield extraction, determined bin by bin for all the three non-strange D mesons are reported in Tables 3 and 5 and in Tables 4 and 6 for D<sub>s</sub><sup>+</sup>.

$p_T$ (GeV/ $c$ )	D <sup>0</sup>	D <sup>+</sup>	D <sup>*+</sup>
1.0-1.5	X	-	-
1.5-2.0	X	-	-
2.0-2.5	X	-	-
2.5-3.0	X	0.05	-
3.0-3.5	X	0.05	0.06
3.5-4.0	X	0.05	0.04
4.0-4.5	X	0.05	0.04
4.5-5.0	X	0.05	0.04
5.0-5.5	X	0.05	0.04
5.5-6.0	X	0.05	0.04
6.0-6.5	X	0.05	0.04
6.5-7.0	X	0.05	0.04
7.0-7.5	X	0.05	0.03
7.5-8.0	X	0.05	0.03
8.0-9.0	X	0.05	0.03
9.0-10.0	X	0.03	0.03
10.0-12.0	X	0.03	0.03
12.0-16.0	X	0.03	0.03
16.0-24.0	X	0.03	0.03
24.0-36.0	X	0.03	0.03
36.0-50.0	X	0.05	0.03

**Table 3:** Systematic uncertainty from yield extraction for the D<sup>0</sup>, D<sup>+</sup> and D<sup>\*+</sup> mesons in the 0–10% centrality class.

$p_T$ (GeV/ $c$ )	D <sub>s</sub> <sup>+</sup>
3.0-4.0	8%
4.0-5.0	8%
5.0-6.0	5%
6.0-8.0	5%
8.0-12.0	3%
12.0-16.0	3%
16.0-24.0	5%
24.0-36.0	5%

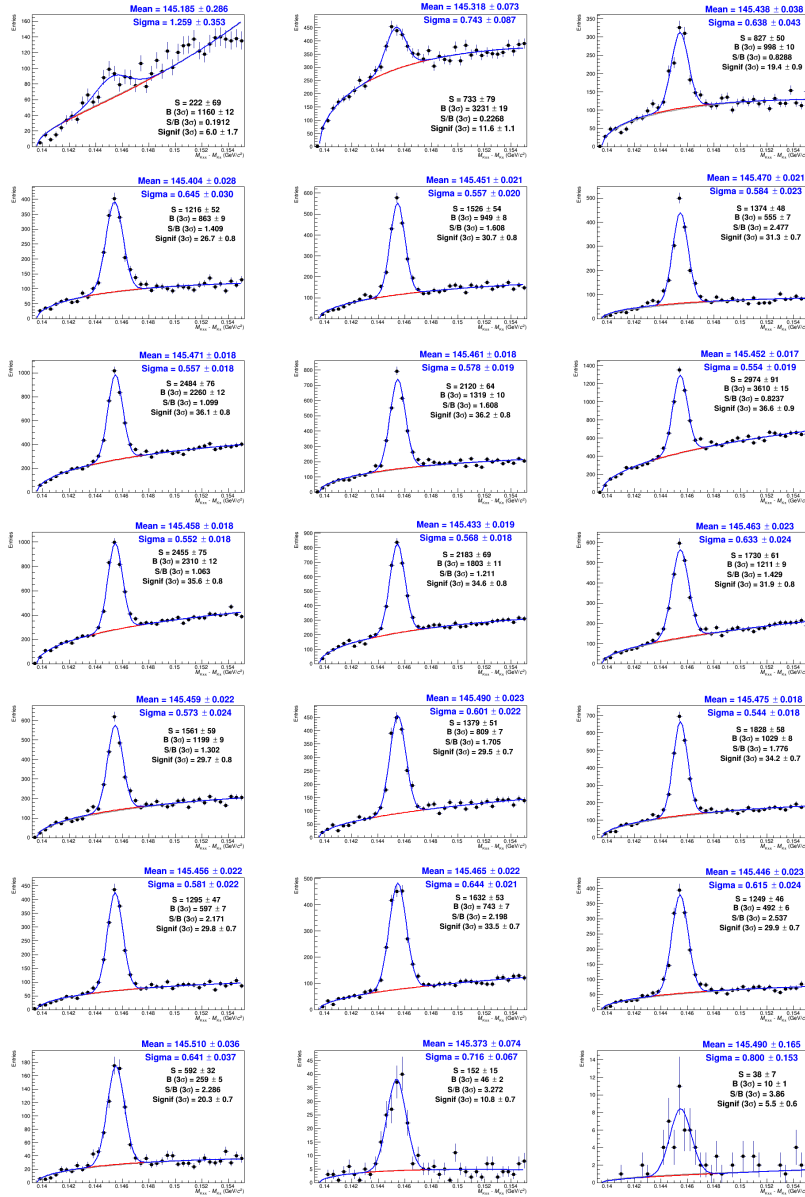
**Table 4:** Systematic uncertainty from yield extraction for the D<sub>s</sub><sup>+</sup> mesons in the 0–10% centrality class.

$p_T$ (GeV/ $c$ )	D <sup>0</sup>	D <sup>+</sup>	D <sup>*+</sup>
1.0-1.5	X	-	-
1.5-2.0	X	-	-
2.0-2.5	X	0.07	0.05
2.5-3.0	X	0.07	0.05
3.0-3.5	X	0.04	0.05
3.5-4.0	X	0.04	0.03
4.0-4.5	X	0.04	0.03
4.5-5.0	X	0.03	0.03
5.0-5.5	X	0.03	0.03
5.5-6.0	X	0.03	0.03
6.0-6.5	X	0.03	0.03
6.5-7.0	X	0.03	0.03
7.0-7.5	X	0.03	0.03
7.5-8.0	X	0.03	0.03
8.0-9.0	X	0.03	0.03
9.0-10.0	X	0.03	0.03
10.0-12.0	X	0.03	0.03
12.0-16.0	X	0.03	0.03
16.0-24.0	X	0.04	0.03
24.0-36.0	X	0.06	0.03
36.0-50.0	X	0.08	-

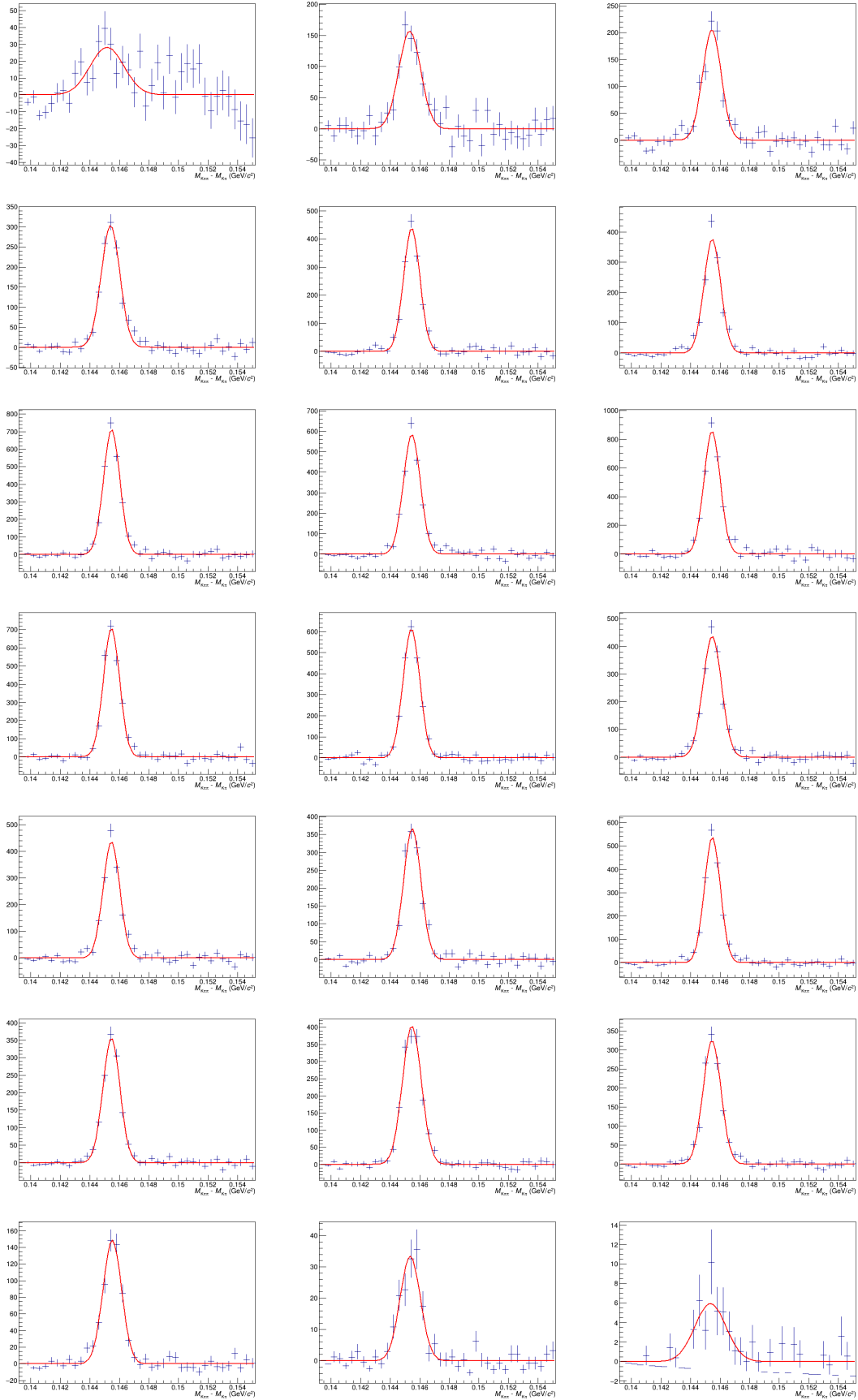
**Table 5:** Systematic uncertainty from yield extraction for the D<sup>0</sup>, D<sup>+</sup> and D<sup>\*+</sup> mesons in the 30–50% centrality class.

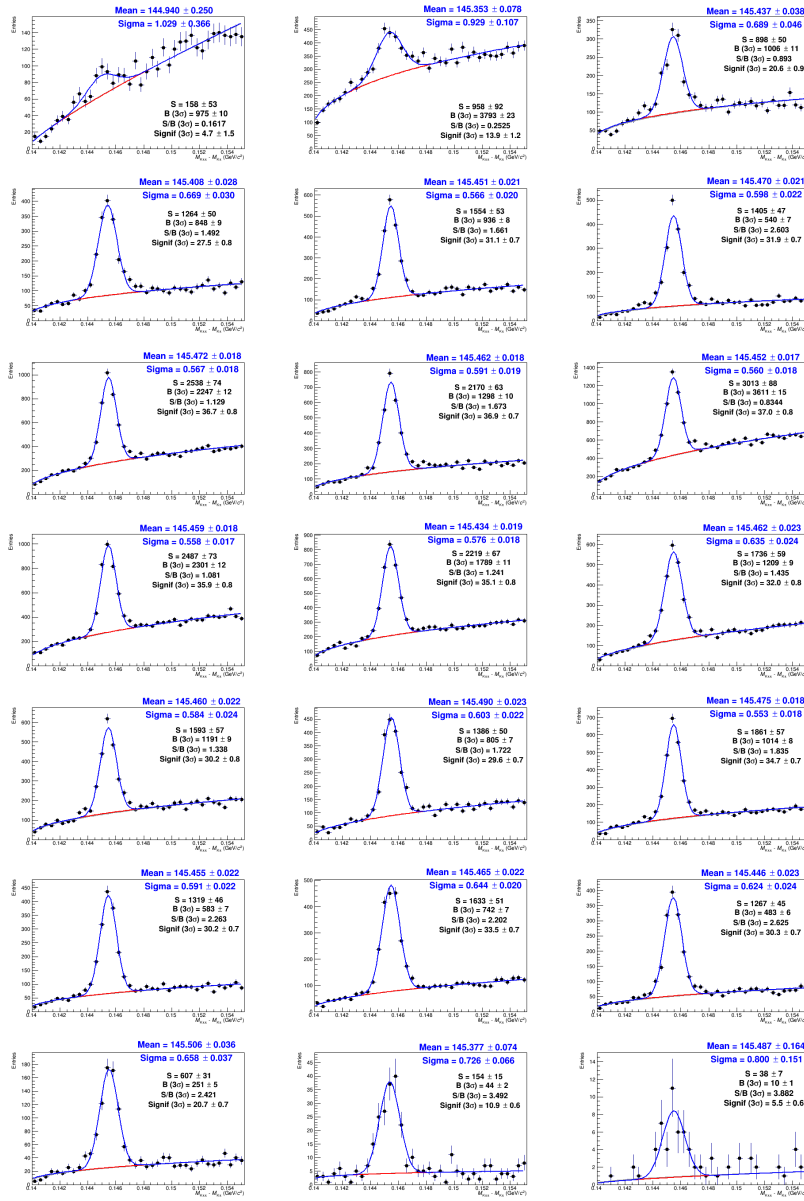
$p_T$ (GeV/ $c$ )	D <sub>s</sub> <sup>+</sup>
3.0-4.0	9%
4.0-6.0	6%
6.0-8.0	4%
8.0-12.0	4%
12.0-16.0	2%
16.0-24.0	3%

**Table 6:** Systematic uncertainty from yield extraction for the D<sub>s</sub><sup>+</sup> mesons in the 30–50% centrality class.

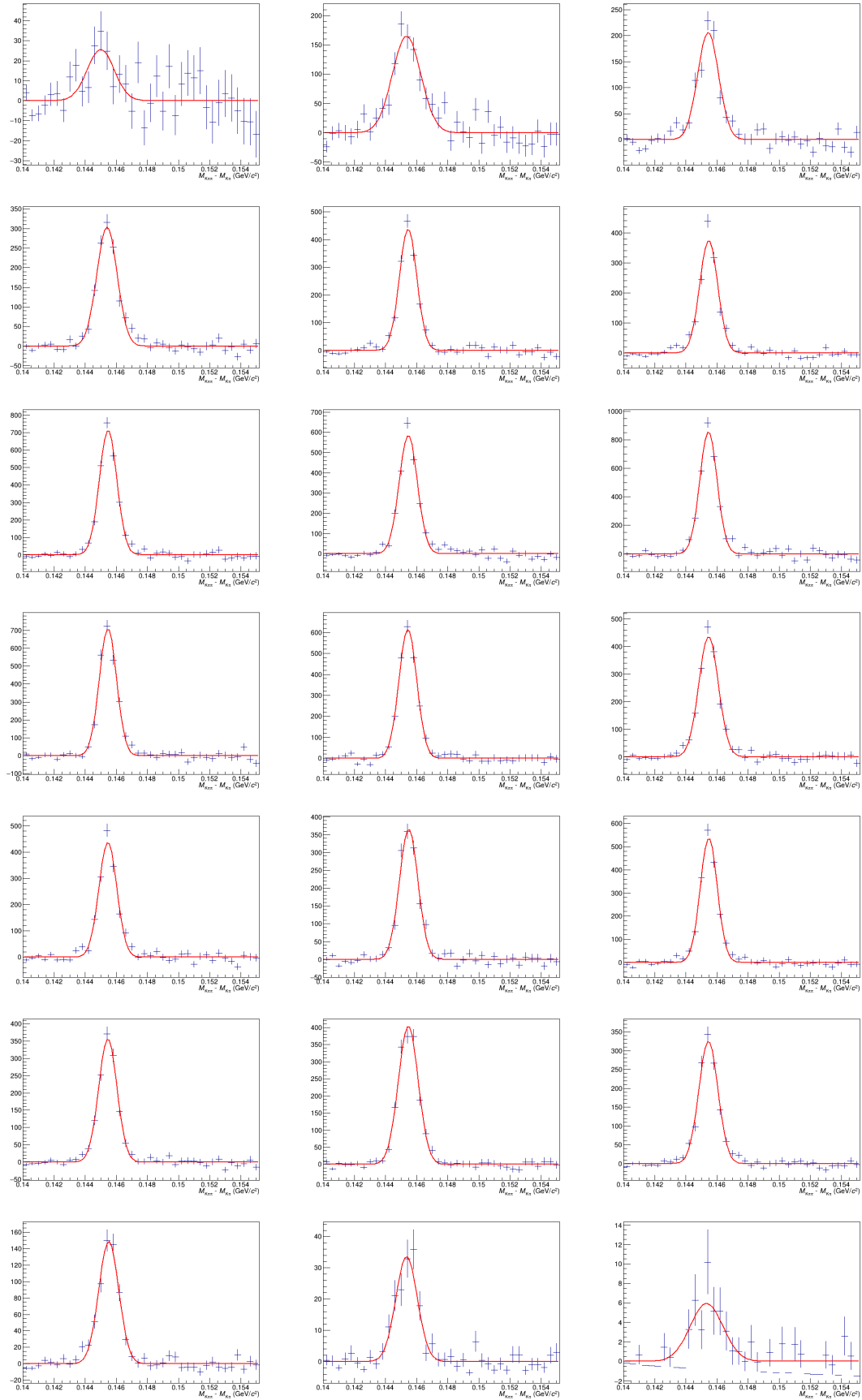


**Fig. 6:**  $D^{*+}$  signal extraction using standard background fit function.

**Fig. 7:** Residual plots using standard background fit function.



**Fig. 8:**  $D^{*+}$  signal extraction using Power fit function for background.

**Fig. 9:** Residual plots using Power fit function for background.

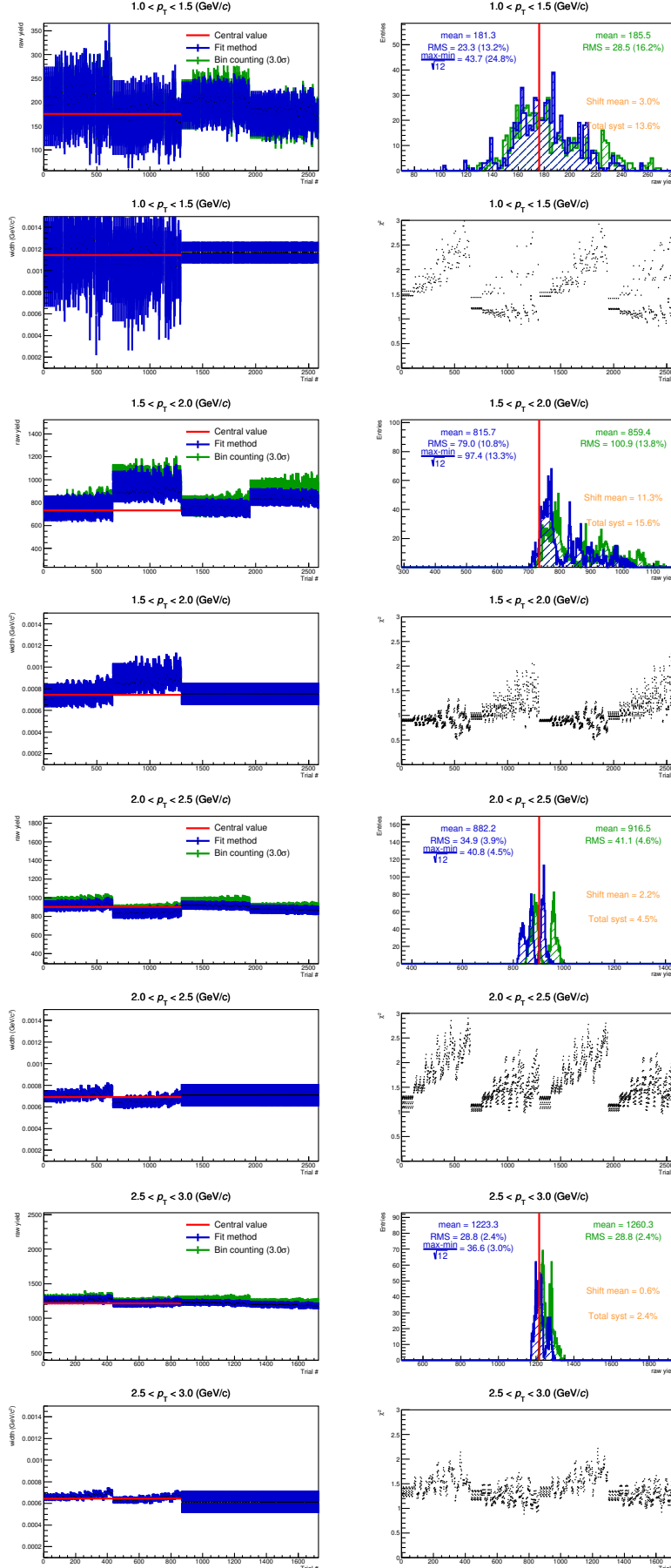


**Fig. 10:** Output of the multi-trial study for  $D^{*+}$  mesons for  $1 < p_T < 3 \text{ GeV}/c$ . For each  $p_T$  bin: the top panel shows the raw yield as a function of trials and raw yield distributions, the bottom panel shows the width and  $\chi^2$  as a function of trials.

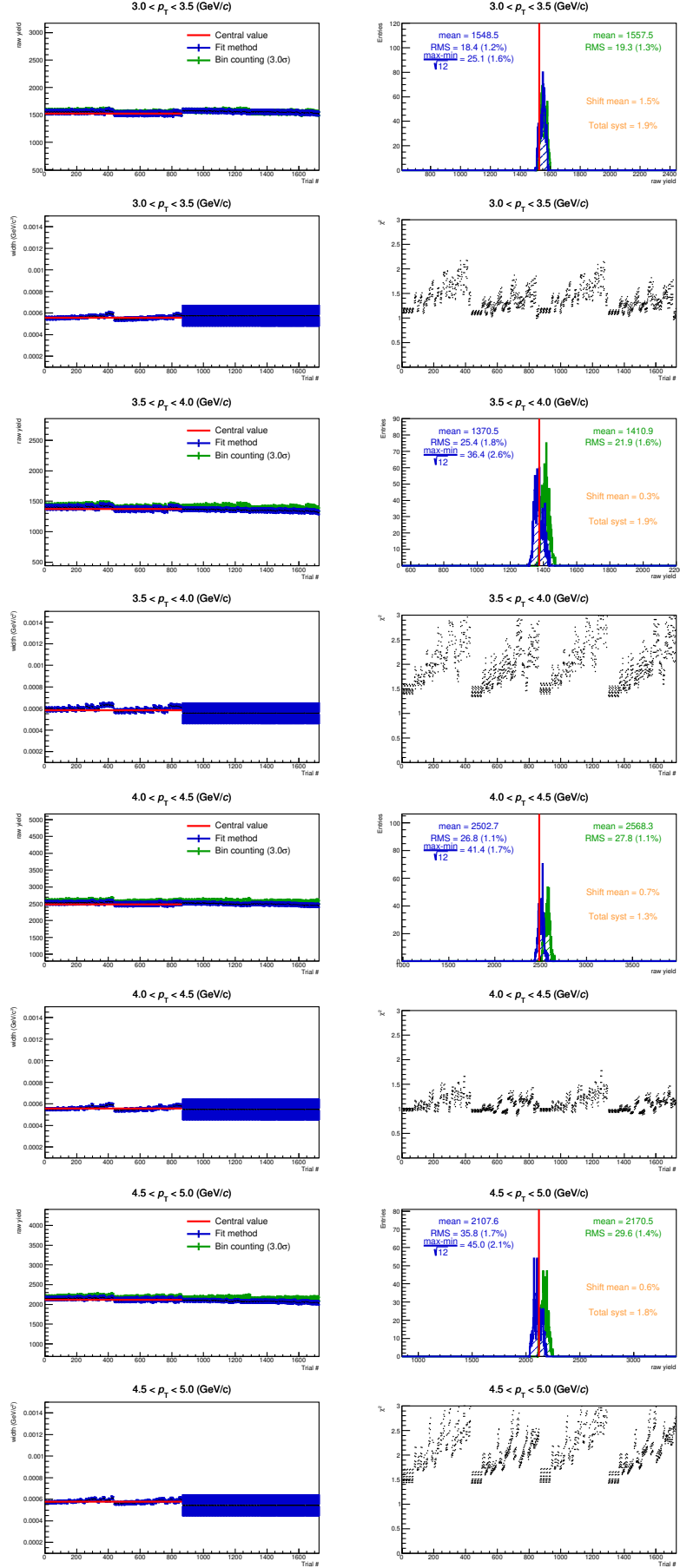


**Fig. 11:** Output of the multi-trial study for D<sup>\*+</sup> mesons for  $3 < p_T < 5$  GeV/c. For each  $p_T$  bin: the top panel shows the raw yield as a function of trials and raw yield distributions, the bottom panel shows the width and  $\chi^2$  as a function of trials.

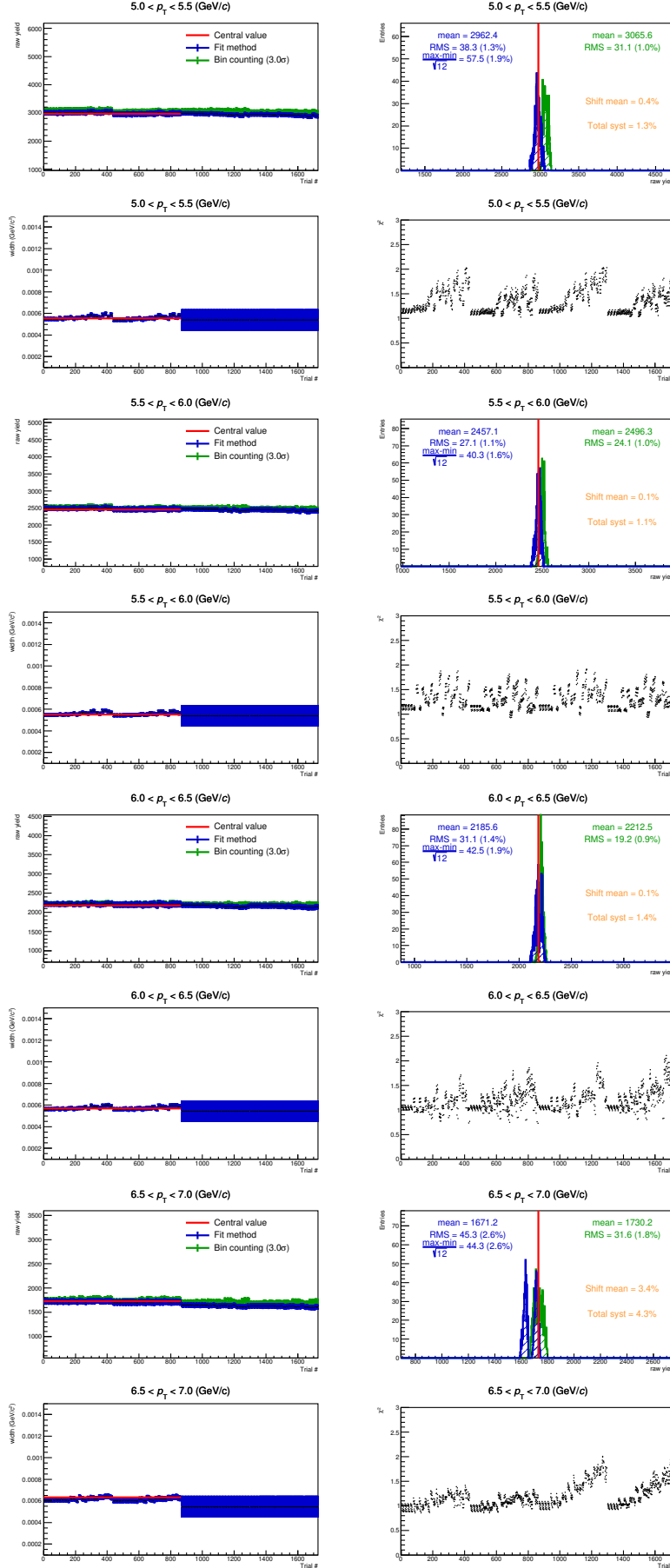


**Fig. 12:** Output of the multi-trial study for  $D^{*+}$  mesons for  $5 < p_T < 7 \text{ GeV}/c$ . For each  $p_T$  bin: the top panel shows the raw yield as a function of trials and raw yield distributions, the bottom panel shows the width and  $\chi^2$  as a function of trials.

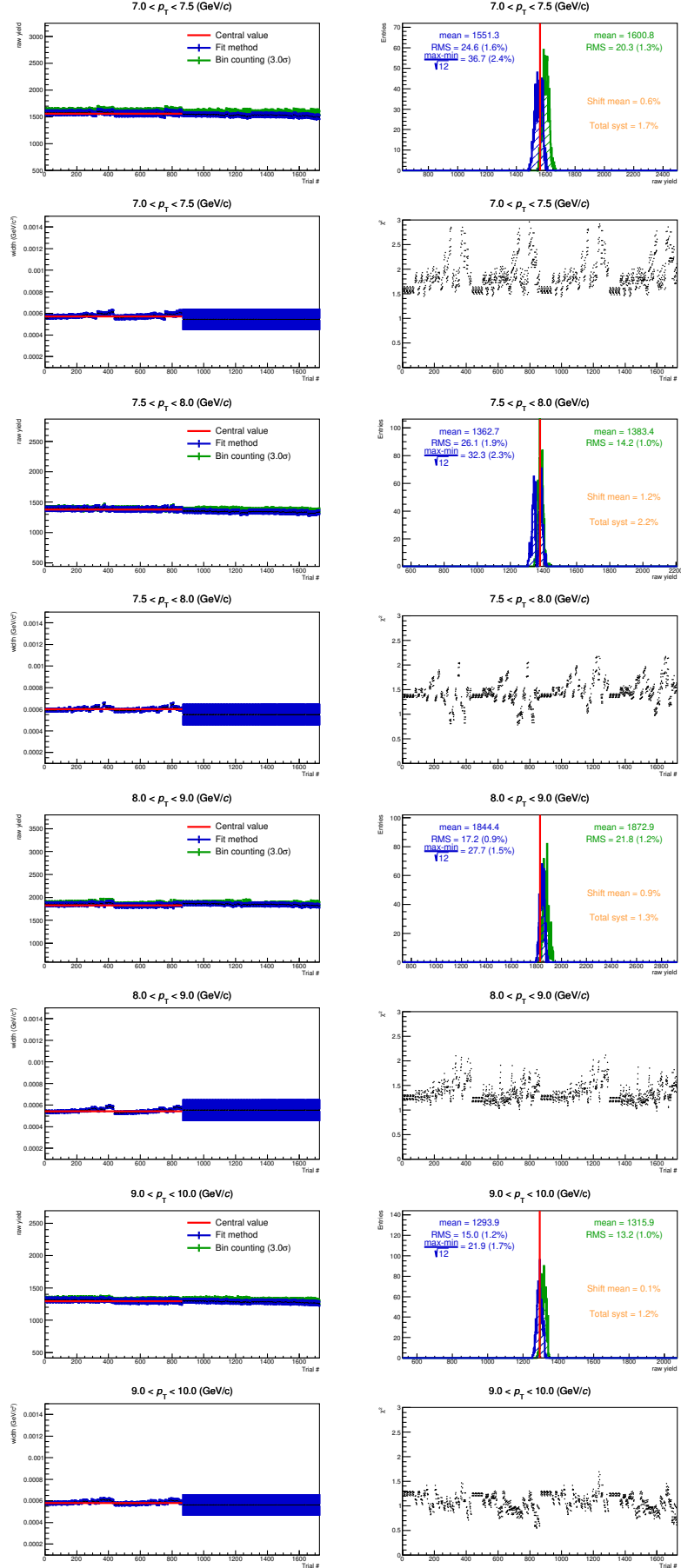


**Fig. 13:** Output of the multi-trial study for D<sup>\*+</sup> mesons for  $7 < p_T < 10$  GeV/c. For each  $p_T$  bin: the top panel shows the raw yield as a function of trials and raw yield distributions, the bottom panel shows the width and  $\chi^2$  as a function of trials.

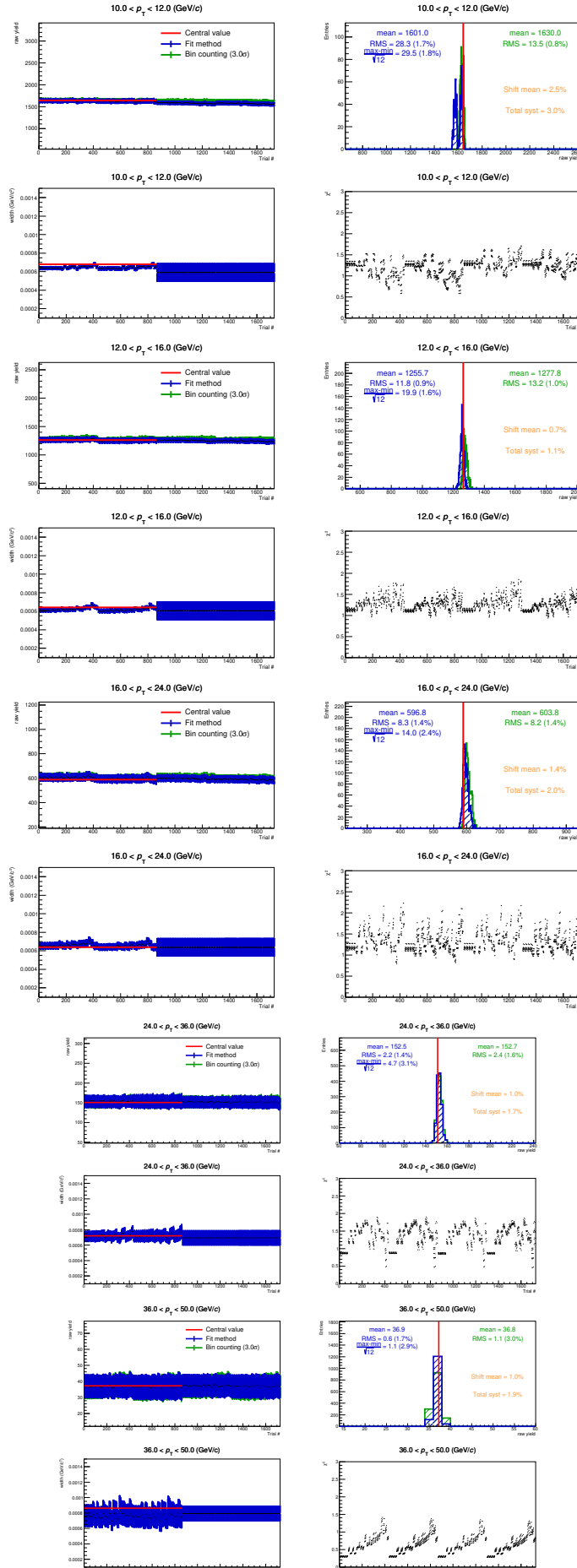


**Fig. 14:** Output of the multi-trial study for  $D^{*+}$  mesons for  $10 < p_T < 50 \text{ GeV}/c$ . For each  $p_T$  bin: the top panel shows the raw yield as a function of trials and raw yield distributions, the bottom panel shows the width and  $\chi^2$  as a function of trials.

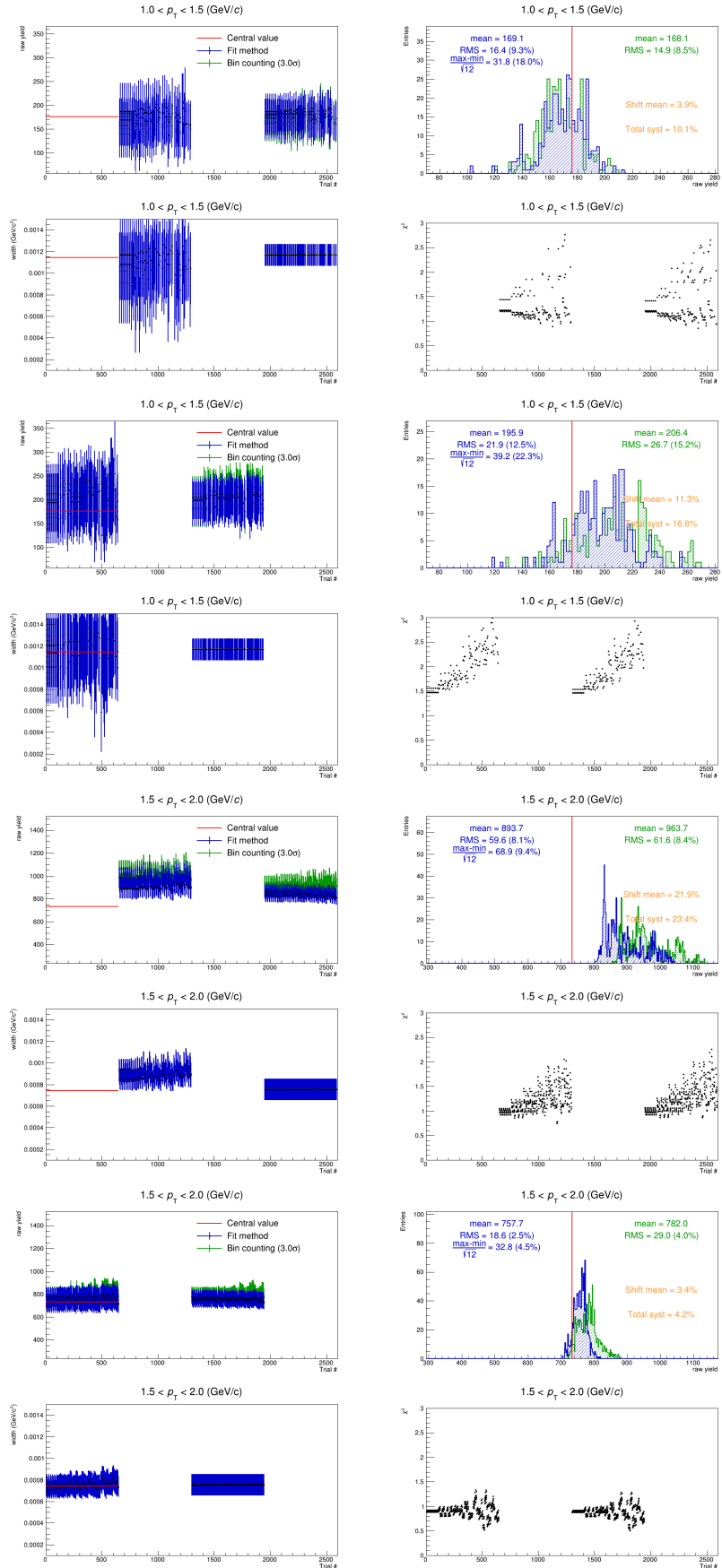


**Fig. 15:** Yield extraction for  $p_T$  1-2 GeV/c tested with only one background function.

## 4.2 Selection efficiency

A further systematic uncertainty can arise from possible differences in the cut-variable shapes in data and Monte Carlo and due to residual misalignment. This sources where checked by repeating the analysis varying the selection cuts from the standard set of cuts. Moving the main cuts all left or all right may introduce a bias due to the fact that all the cuts goes in the same direction. Due to this concern, different sets of cuts, alternative to the standard one were tested.

For the  $D_s^+$  meson, a systematic scan from loose to tight cuts was done on a variable per variable basis, reconstructing the yields, comparing them to the yields obtained with a reference set of cuts and looking for possible trends/biases of the reconstructed yield as a function of the cut strength. The result of this study for each  $p_T$  bin is shown n Figs. ?? and ??, where the variations of the raw yield, prompt and feed-down  $D_s^+$  efficiency, significance, signal-to-background ratio, and corrected yield are plotted as a function of the cut set tested. Finally the distribution of the variation of the corrected yield is shown. All the trials for which the extracted yield had a significance larger than 3 and a variation of the efficiency larger than 1% were taken into account. The systematic uncertainty was assigned considering the rms and the deviation from unity of these distributions. The values are reported in Table ??.

For the  $D^{*+}$  meson, a systematic scan from loose to tight cuts was done by varying the variables: dca,  $d0 \times d0$ ,  $p_T$  kaon and  $p_T$  pion. The result of this study is shown in Figs. 16 and ??, where the variation of the rawyield, prompt efficiency, and corrected yield ratio are plotted as a function of the cut set tested.

For the  $D^+$  meson, a systematic scan from loose to tight cuts was done by varying the variables. The result of this study is shown in Figs. ?? and ??, where the variation of the rawyield, prompt efficiency, and corrected yield ratio are plotted as a function of the cut set tested.

$p_T$ (GeV/c)	$D^0$	$D^+$	$D^{*+}$
1.0-1.5	X	-	-
1.5-2.0	X	-	-
2.0-2.5	X	-	-
2.5-3.0	X	10	-
3.0-3.5	X	6	12%
3.5-4.0	X	6	10%
4.0-4.5	X	6	10%
4.5-5.0	X	6	10%
5.0-5.5	X	6	8%
5.5-6.0	X	5	8%
6.0-6.5	X	5	8%
6.5-7.0	X	4	8%
7.0-7.5	X	4	8%
7.5-8.0	X	4	8%
8.0-9.0	X	3	8%
9.0-10.0	X	3	8%
10.0-12.0	X	3	6%
12.0-16.0	X	3	4%
16.0-24.0	X	3	4%
24.0-36.0	X	4	4%
36.0-50.0	X	4	2%

**Table 7:** Systematic uncertainty estimated with the cut-variation study for the  $D^0$ ,  $D^+$ , and  $D^{*+}$  mesons in the 0–10% centrality class.

$p_T$ (GeV/ $c$ )	D <sup>0</sup>	D <sup>+</sup>	D <sup>*+</sup>
1.0-1.5	X	-	-
1.5-2.0	X	-	-
2.0-2.5	X	7	18%
2.5-3.0	X	5	6%
3.0-3.5	X	5	6%
3.5-4.0	X	4	6%
4.0-4.5	X	4	6%
4.5-5.0	X	4	6%
5.0-5.5	X	4	6%
5.5-6.0	X	4	6%
6.0-6.5	X	2	6%
6.5-7.0	X	2	6%
7.0-7.5	X	2	6%
7.5-8.0	X	2	6%
8.0-9.0	X	2	6%
9.0-10.0	X	2	2%
10.0-12.0	X	2	0
12.0-16.0	X	2	0
16.0-24.0	X	2	0
24.0-36.0	X	4	0
36.0-50.0	X	6	-

**Table 8:** Systematic uncertainty estimated with the cut-variation study for the D<sup>0</sup>, D<sup>+</sup>, and D<sup>\*+</sup> mesons in the 30–50% centrality class.

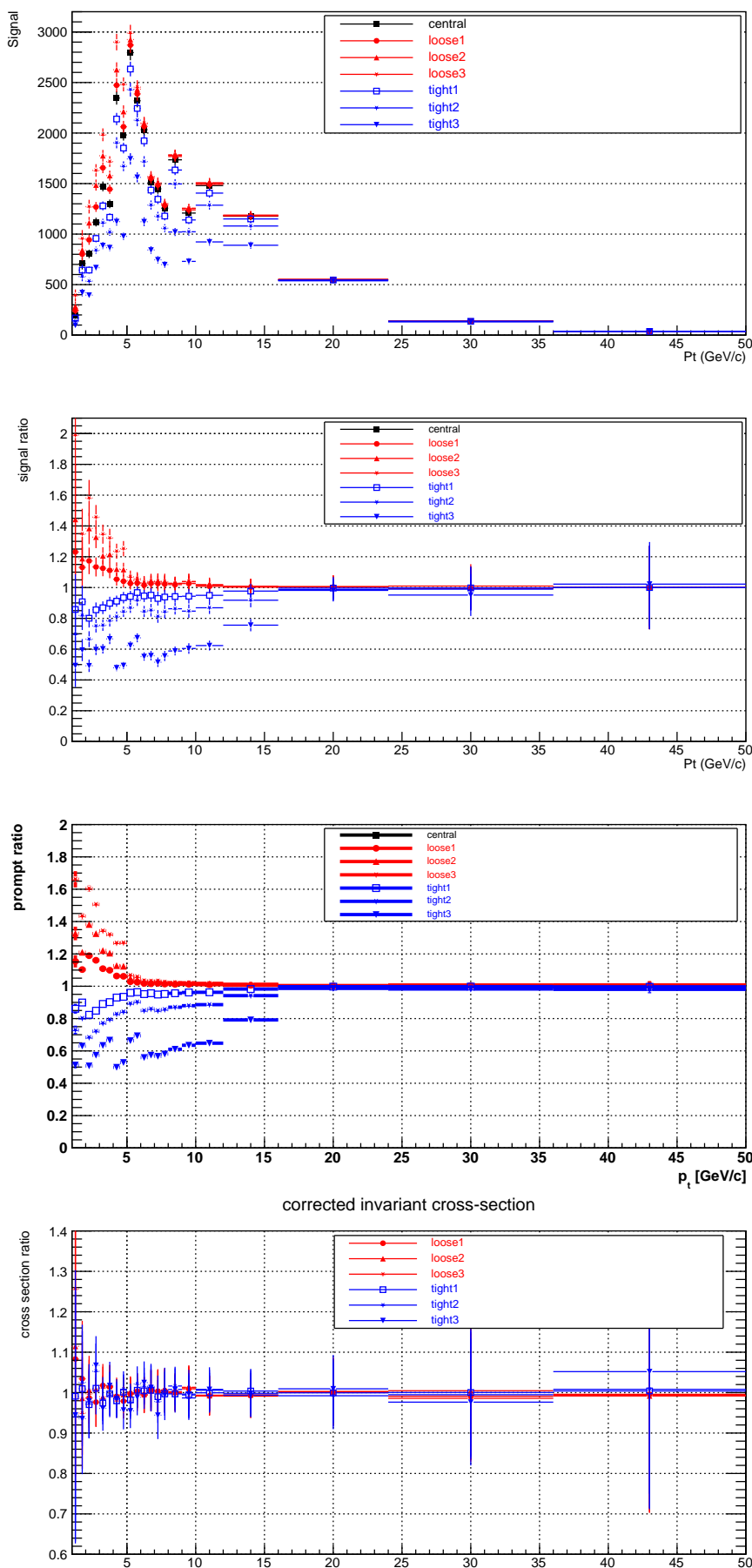


**Fig. 16:** Variations of raw yield, prompt efficiency, and corrected yield obtained with the cut-variation study for the  $D^{*+}$  mesons in the 0–10% centrality class.

### 4.3 Generated $p_T$ shape

Another source of systematic we investigated is the one arising from the D meson  $p_T$  shape assumed in the Monte Carlo used for corrections. In our simulation the D mesons are folded in the HIJING event using PYTHIA and as a result the  $p_T$  shape of the D mesons can be biased leading to an effect in the final efficiency used for corrections. In order to check the stability of our efficiencies against the change in  $p_T$  shape and to define a systematic uncertainty it was decided to implement several set of weights.

For the D<sub>s</sub><sup>+</sup> meson, the  $p_T$  shapes provided by different models were taken into account. For the default value, the  $p_T$  shape of TAMU was considered, since it implements both the in-medium energy loss and the enhanced D<sub>s</sub><sup>+</sup> production due to the hadronisation via coalescence in a strange-rich medium. For the variation, the shapes of PHSD, Catania models, which also provide predictions for the D<sub>s</sub><sup>+</sup> mesons were considered. In addition, the MC@sHQ model for non-strange D mesons was considered to take into account a scenario in which the D<sub>s</sub><sup>+</sup> is not enhanced and as extreme case FONLL that assumes no suppression.

The  $p_T$  shapes and the corresponding  $p_T$  weights, obtained by dividing each shape by the one of the MC simulation, are reported in Fig. ?? and Fig. ?? for the 0–10% and 30–50% centrality classes. The variation of the efficiency of prompt D<sub>s</sub><sup>+</sup> mesons is reported in Fig. ?? and Fig. ???. For the 0–10% centrality class, 2% systematic was assigned in the range  $3 < p_T < 12$  GeV/c, while no systematic uncertainty was assigned for  $p_T > 12$  GeV/c. For the 30–50% centrality class, 3% systematic was assigned in the range  $3 < p_T < 6$  GeV/c, 1% in the range  $8 < p_T < 12$  GeV/c while no systematic uncertainty was assigned for  $p_T > 12$  GeV/c.

For the non-strange D mesons 0–10% centrality class, the re-weighted shape was obtained from the mixture of the measured D<sup>0</sup> corrected yield shape with FONLL predictions, used in  $p_T$  regions where the measurement is not feasible or not precise. Then, other  $p_T$  weight was considered to check the stability of the efficiencies against the  $p_T$  shape of the generated D mesons. For the 0–10% centrality class, the systematic uncertainty was evaluated comparing the central values of the efficiency obtained using the FONLL times LBT. For the 30–50% centrality class, the systematic uncertainty was evaluated comparing the central values of the efficiency (applying FONLL5andBAMPS weight) to that obtained applying the FONLL weight.

$p_T$ (GeV/ $c$ )	$D^0$	$D^+$	$D^{*+}$
1.0-1.5	X	-	-
1.5-2.0	X	-	-
2.0-2.5	X	-	-
2.5-3.0	X	2	-
3.0-3.5	X	1	1%
3.5-4.0	X	1	0.5%
4.0-4.5	X	1	0
4.5-5.0	X	1	0
5.0-5.5	X	0	0
5.5-6.0	X	0	0
6.0-6.5	X	0	0
6.5-7.0	X	0	0
7.0-7.5	X	0	0
7.5-8.0	X	0	0
8.0-9.0	X	0	0
9.0-10.0	X	0	0
10.0-12.0	X	0	0
12.0-16.0	X	0	0
16.0-24.0	X	0	0
24.0-36.0	X	0	0
36.0-50.0	X	0	-

**Table 9:** Systematic uncertainty estimated with the MC  $p_T$  shape study for the  $D^0$ ,  $D^+$ , and  $D^{*+}$  mesons in the 0–10% centrality class.

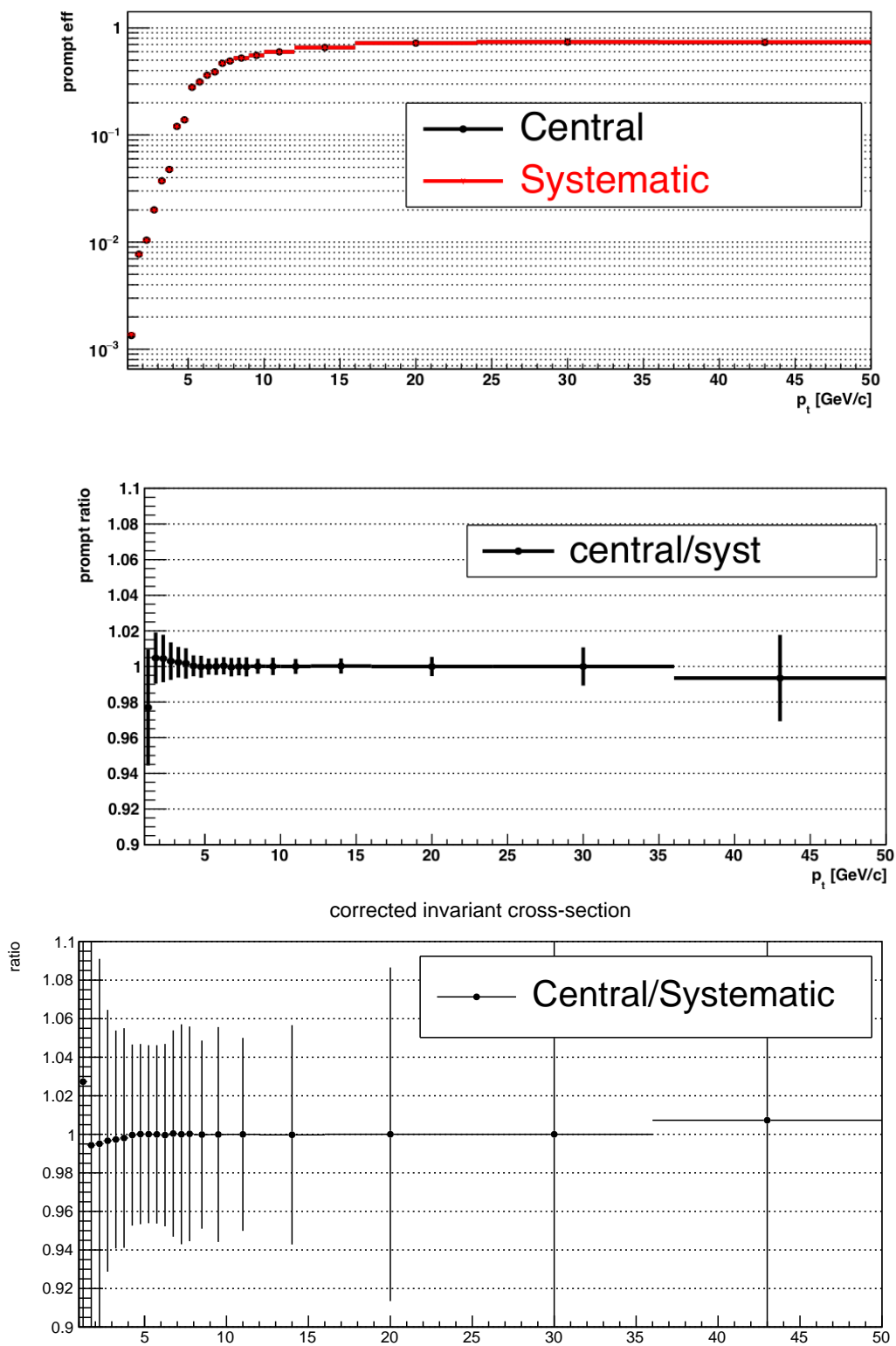


**Fig. 17:** Relative change in efficiencies by using PYTHIA8 (central) with respect to FONLL5anddata (systematic) weight.

#### 4.4 PID efficiency

The systematic uncertainty on the PID selection efficiency was evaluated with a per-track study, using relatively pure samples of pions and kaons. Pions were selected from  $K_s^0$  and  $\Lambda$  decays, while kaons in the TPC (TOF) were selected applying a tight selection on the PID signal in the TOF (TPC) of  $|N_\sigma(K)| < 0.2$ .

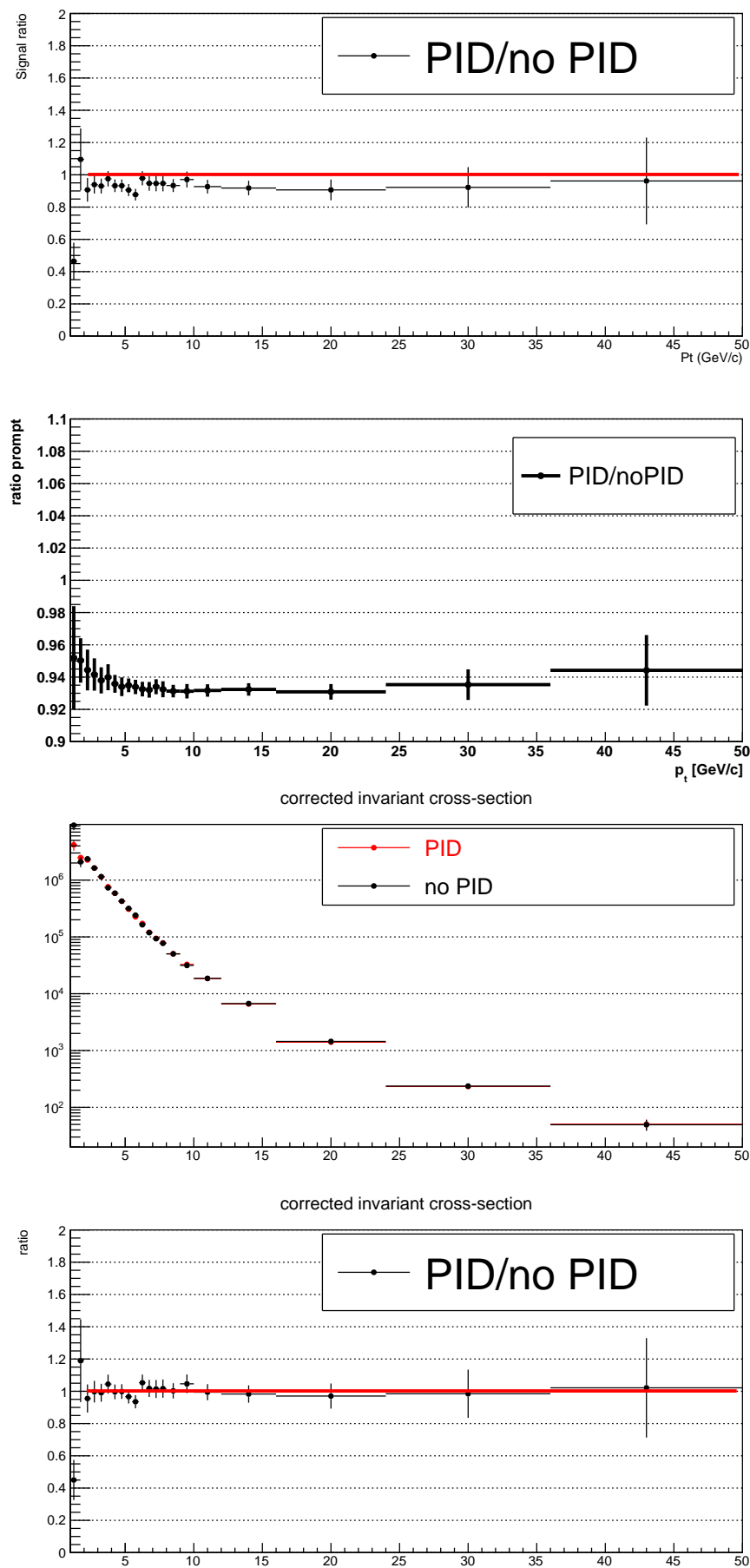
However, for this data sample, a discrepancy between the TPC PID efficiency in data and MC simulation up to 5%, 15%, 30% for a  $3\sigma$ ,  $2\sigma$ , and  $1\sigma$  selection, respectively, was observed. This was caused by an imperfect calibration of the expected  $dE/dx$  for the different hadron species in the data, which was reflected in a deviation of the  $N_\sigma^{\text{TPC}}$  distributions from the Normal distribution. In order to avoid large biases in the D-meson measurement, a post-calibration procedure was applied to correct the  $N_\sigma^{\text{TPC}}$  values. In particular, the distributions obtained from the pure samples of pions and kaons were fitted with a Gaussian function to extract the mean,  $\langle N_\sigma^{\text{TPC}} \rangle$ , and the width,  $\sigma(N_\sigma^{\text{TPC}})$ , of the uncalibrated distributions of pions and kaons. The extracted parameters were then used to compute the corrected  $N_\sigma^{\text{TPC,corr}}$  value for each track as

$$N_\sigma^{\text{TPC,corr}}(X) = \frac{N_\sigma^{\text{TPC}}(X) - \langle N_\sigma^{\text{TPC}}(X) \rangle}{\sigma(N_\sigma^{\text{TPC}}(X))}, \quad (3)$$

where  $X$  stands for a given mass hypothesis, i.e. pion or kaon. This procedure was performed in intervals of track momentum and pseudorapidity. Figures 18 and ?? show the  $N_\sigma^{\text{TPC}}$  distributions as a function of pseudorapidity before the post calibration for the LHC18q and LHC18r periods, respectively, while Fig. ?? after the post-calibration for both the periods for the 0–10% centrality class. Samples of pions, kaons and protons independent of the one used to compute the correction were used to cross check the goodness of the post-calibration. The mean value of the distribution before the correction is shifted towards negative values, and shows a clear  $\eta$ -dependence. The corrected distribution is constantly centred at zero as a function of  $\eta$ . The residual deviation from unity in the kaon and proton distributions is due to residual contamination in the samples.

In Figs. ?? and ?? the data-to-MC ratios of the  $N_\sigma^{\text{TPC}}$  and  $N_\sigma^{\text{TOF}}$  selection efficiencies of pions and kaons as a function of  $p_T$  in the 0–10% centrality class for a  $3\sigma$ ,  $2\sigma$ , and  $1\sigma$  selection after the TPC recalibration procedure. A similar result was obtained in the 30–50% centrality class. The deviation from unity of these ratios was considered as systematic uncertainty on the single track.

The single-track systematic uncertainty was propagated to the D mesons using the decay kinematics of the MC simulation used for the analysis. Figs. ??, ?? and ?? show the systematic uncertainty obtained for the  $D_s^+$  and  $D^0$  mesons in the 0–10% centrality class. The uncertainty for the conservative PID strategy was assigned to the  $D_s^+$ -meson measurement for  $p_T < 8 \text{ GeV}/c$ , while that for the strong PID strategy at higher  $p_T$ .

**Fig. 18:** PID systematic D<sup>\*+</sup> meson.

## 4.5 Track reconstruction efficiency

The systematic uncertainty due to the track-reconstruction efficiency includes the contributions of the track-finding procedure in the TPC detector and prolongation in the ITS detector, and the track-quality selections.

The ITS-TPC matching efficiency was computed as the number of tracks successfully fitted with the Kalman filter in the TPC and ITS, with at least one hit in the SPD layers, divided by the number of reconstructed tracks successfully fitted in the TPC. The systematic uncertainty on its determination arises from discrepancies in the tracking performance between data and the MC simulation. The ITS-TPC matching efficiency is different for particles produced in the collision, including strong decays and weak decays of charm and beauty hadrons, which are considered as primary particles in this study, and secondary particles (i.e. particles produced in the interactions with the material or in decays of strange hadrons). The HIJING event generator and the GEANT3 transport package do not reproduce the relative abundance of primary and secondary particles, therefore data-driven corrections for the fraction of primary particles ( $f_{\text{primary}}$ ) were used to weight the MC simulation and obtain the corrected inclusive MC efficiency ( $\epsilon_{\text{inclusive}}(\text{MC})$ ), which is computed as:

$$\epsilon_{\text{inclusive}}(\text{MC}) = f_{\text{primary}} \cdot \epsilon_{\text{primary}}(\text{MC}) + (1 - f_{\text{primary}}) \cdot \epsilon_{\text{secondary}}(\text{MC}), \quad (4)$$

where  $\epsilon_{\text{primary}}(\text{MC})$  and  $\epsilon_{\text{secondary}}(\text{MC})$  are the ITS-TPC matching efficiencies for primary and secondary particles, which are determined via fits to the  $d_0^{xy}$  distributions of the tracks.

In addition, it was checked if a discrepancy between the efficiency of the track-quality selections in data and in the MC simulation need to be considered. For this purpose, the D-meson cross section was re-evaluated with three alternative track-quality selection criteria, which include the selection of tracks with (i) a number TPC crossed rows larger than  $120 - 5/(p_T [\text{GeV}/c])$  instead of the default value of 70, (ii) the number of TPC clusters at least 0.65 times the number of TPC crossed rows and (iii) a ratio of crossed rows over findable clusters in the TPC larger than 0.9 (being the default 0.8). These variations are shown for the  $D_s^+$  meson in the 0–10% centrality class in Fig. ???. The variation of the cross section was observed to be around 1.0% for  $D^0$  (two-body decay) and 1.5% for the other D mesons (three-body decays), therefore a value equal to 0.5% was added to the per-track systematic uncertainty estimated for the ITS-TPC matching efficiency.

Finally, the  $p_T$ -dependent per-track systematic uncertainty was propagated to the  $D_s^+$  mesons via the kinematics of the  $D_s^+$  daughter tracks, similarly to the procedure explained in the previous Section for the PID uncertainty. The systematic uncertainties obtained for  $D_s^+$  and  $D^0$  mesons in the 0–10% centrality class are shown in Figs. ?? and 20.

## 5 Feed-down subtraction

The feed-down contribution was estimated using the beauty production cross section from the FONLL calculation, the  $B \rightarrow D$  decay kinematics from the EvtGen package, and the Monte Carlo efficiencies for feed-down D mesons. Thus, omitting for brevity the symbol of the  $p_T$ -dependence ( $p_T$ ), the fraction of prompt D mesons reads:

$$\begin{aligned} f_{\text{prompt}} &= 1 - (N^D \text{ feed-down raw} / N^D \text{ raw}) \\ &= 1 - \left( \frac{d^2\sigma}{dy dp_T} \right)_{\text{feed-down}}^{\text{FONLL}} \cdot \frac{(Acc \times \epsilon)_{\text{feed-down}} \cdot \Delta y \Delta p_T \cdot BR \cdot L_{\text{int}}}{N^D \text{ raw} / 2}, \end{aligned} \quad (5)$$

where  $(Acc \times \epsilon)_{\text{feed-down}}$  is the acceptance-times-efficiency for feed-down D mesons and the factor 2 at the denominator comes for counting both particle and antiparticle are combined while in FONLL not. The nuclear modification factor of the feed-down D mesons,  $R_{AA}^{\text{feed-down}}$ , is related to the nuclear

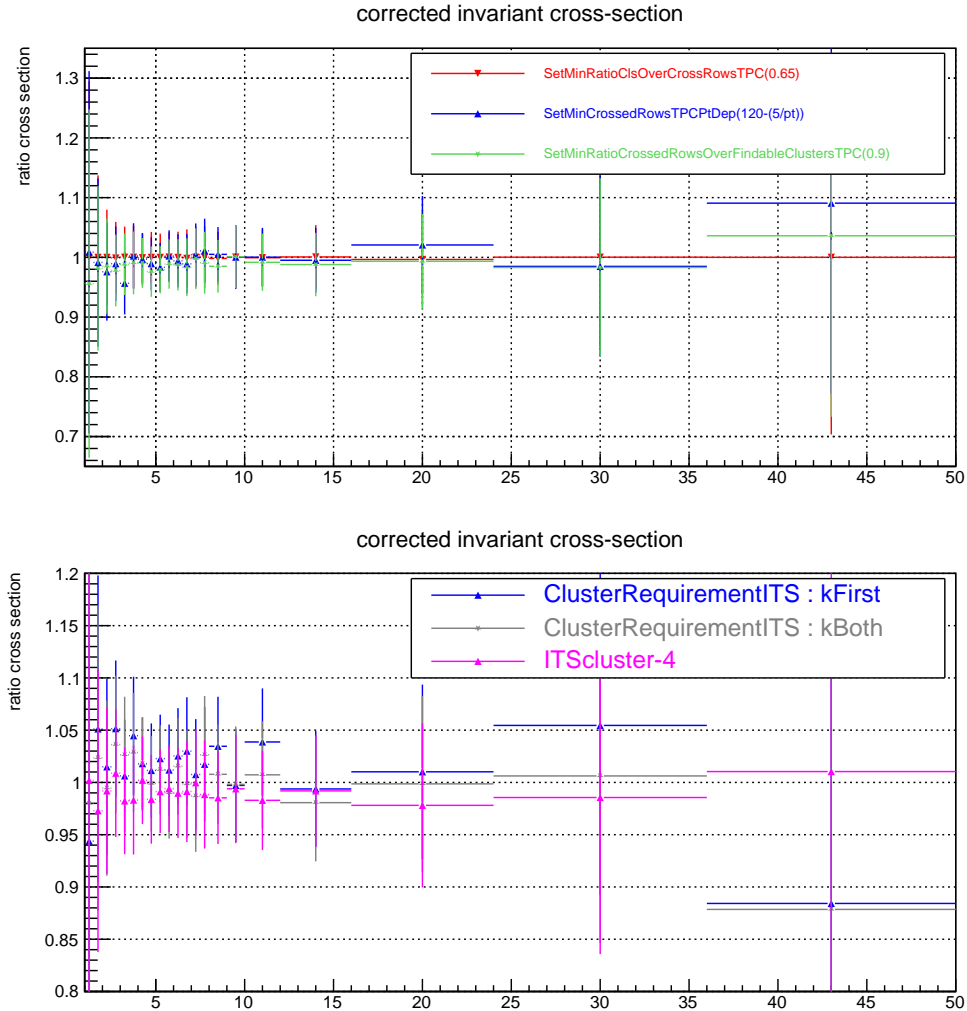


**Fig. 19:** Comparison of D<sup>\*+</sup> corrected yield measured obtained with different TPC track-quality criteria.

modification of beauty production in Pb–Pb collisions, which is currently unknown. Taking advantage of the recent non-prompt J/ $\Psi$  results from the CMS collaboration we assumed for the correction that the nuclear modification factor for feed-down is equal to two times the one of the prompt D mesons ( $R_{AA}^{\text{feed-down}} = 2R_{AA}^{\text{prompt}}$ ) and varied this hypothesis in the range  $1 < R_{AA}^{\text{feed-down}}/R_{AA}^{\text{prompt}} < 3$  ( $1/3 < R_{AA}^{\text{feed-down}}/R_{AA}^{\text{prompt}} < 3$  for D<sub>s</sub><sup>+</sup>) to determine the systematic uncertainty. In the left panel of Fig. ?? (Fig. ??) the variation of  $R_{AA}^{\text{prompt}}$  for D<sub>s</sub><sup>+</sup> mesons in the 0–10% (30–50%) centrality class is shown as a function of this hypothesis for some (all)  $p_T$  intervals of the analysis. The resulting fraction of prompt D<sub>s</sub><sup>+</sup> in the same centrality class is reported in the right panel of the same figure. In Fig. ?? and ?? the variation of  $R_{AA}^{\text{prompt}}$  for D<sup>0</sup> mesons in the 0–10% and 30–50% centrality classes are reported as a function of this hypothesis for some  $p_T$  intervals of the analysis in the left panel of each figure. The resulting fraction of prompt D<sup>0</sup> in the same centrality classes are reported as line histogram in the right panel of the Fig. ?? and ?. In addition, to estimate the systematic uncertainty, the perturbative uncertainty on the FONLL beauty production cross section was considered, by varying the b quark mass and the factorization and renormalization scales as suggested in [6].

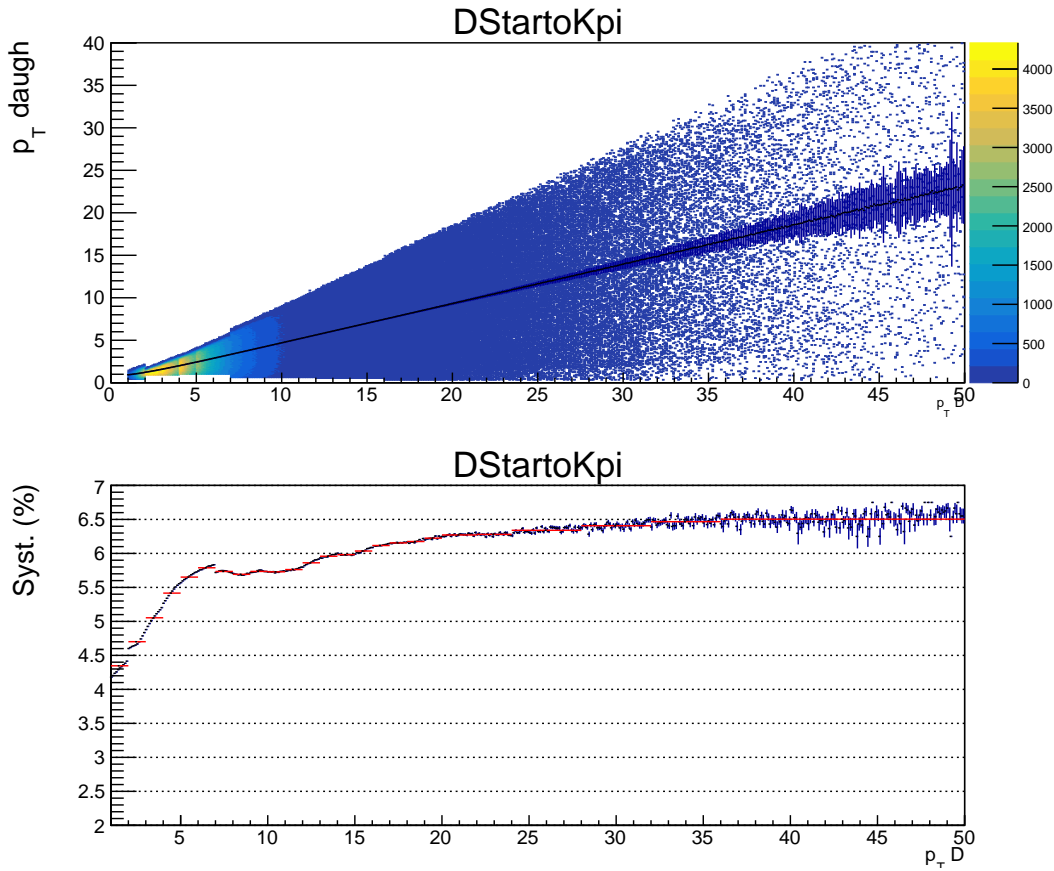


**Fig. 20:** Systematic uncertainty on tracking efficiency assigned to  $D^{*+}$  mesons.

## 6 Results

In this Section, the  $D^{*+}$  production cross sections are shown in Fig. 23. Figure 24 shows the comparison between the new analysis with full data sample 2016, 2017 and 2018 with respect to the old analysis only with 2016 data. The  $p_T$ -differential cross section of prompt  $D^{*+}$  is compared to theoretical model, FONLL, is shown in Fig. 25.

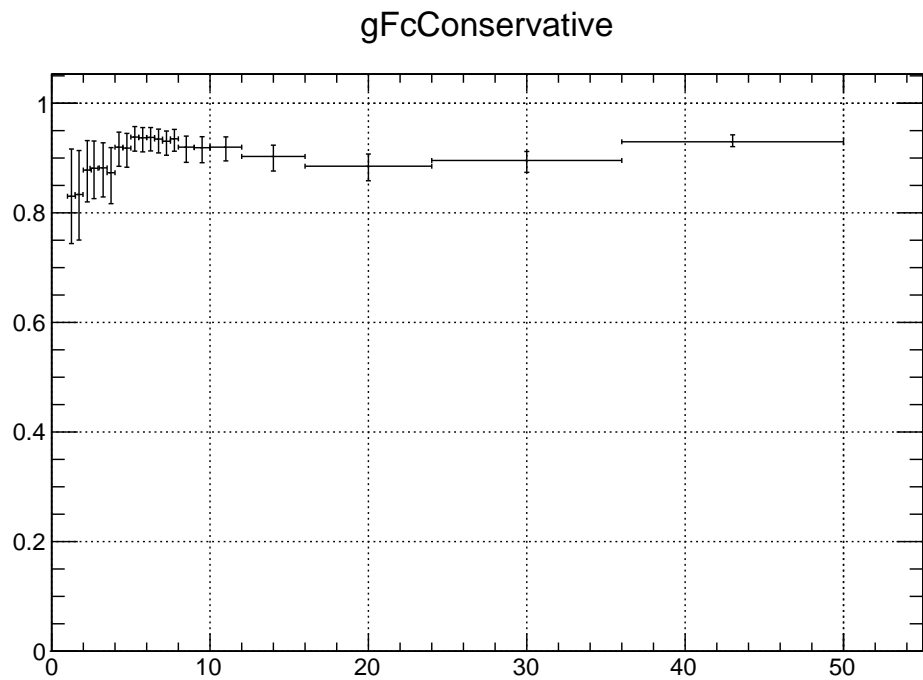


**Fig. 21:** Fraction of prompt D<sup>\*+</sup> estimated using the FONLL-based approach.

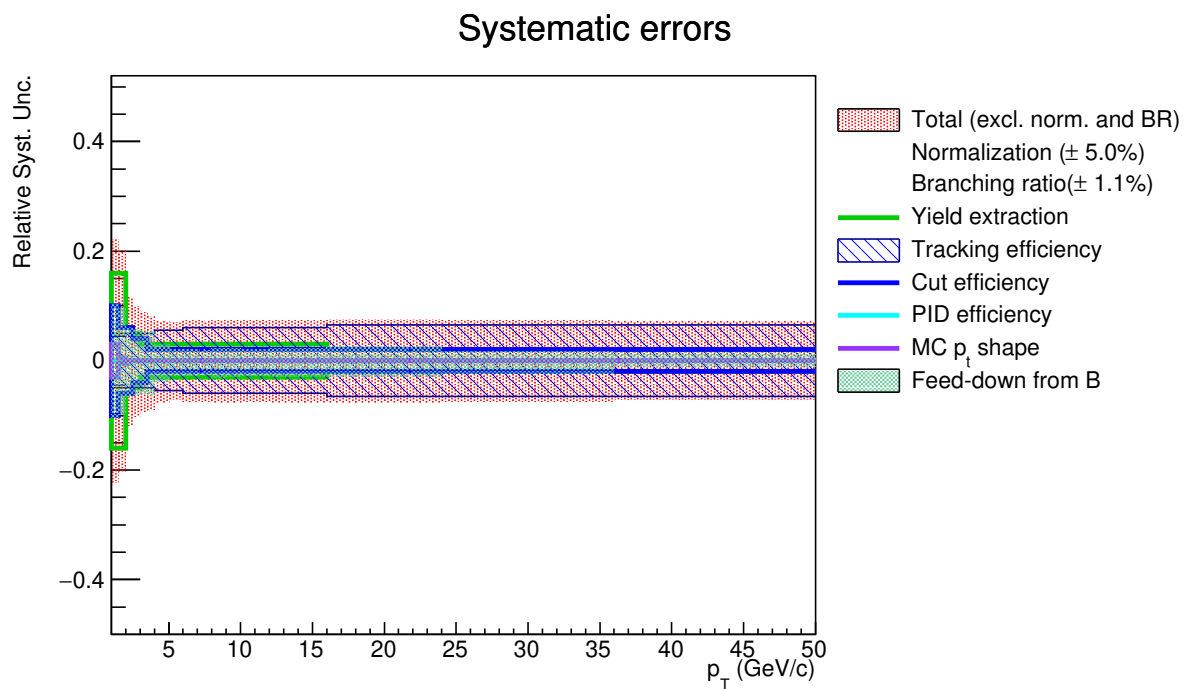


**Fig. 22:** Relative systematic uncertainties on the  $p_T$ -differential production cross section of prompt D<sup>\*+</sup> mesons.

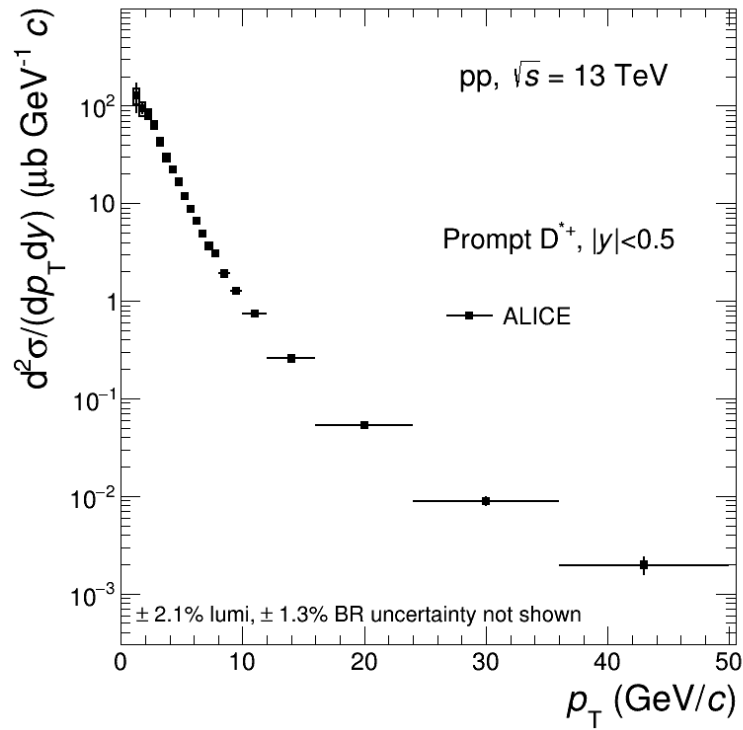


**Fig. 23:**  $p_T$ -differential inclusive production cross section of prompt  $D^{*+}$  mesons in pp collisions at  $\sqrt{s} = 13 \text{ TeV}$ .

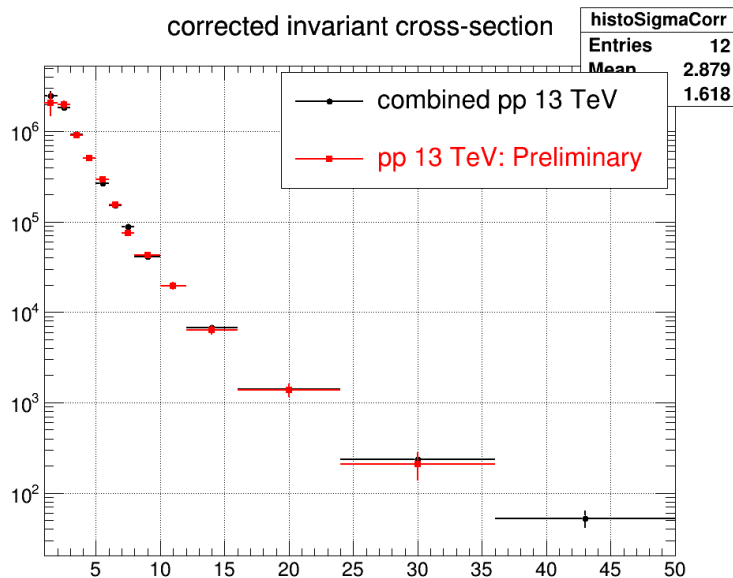


**Fig. 24:** Comparison new analysis full data sample (2016, 2017 and 2018) with respect to the only 2016 data in pp collisions at  $\sqrt{s} = 13 \text{ TeV}$ .

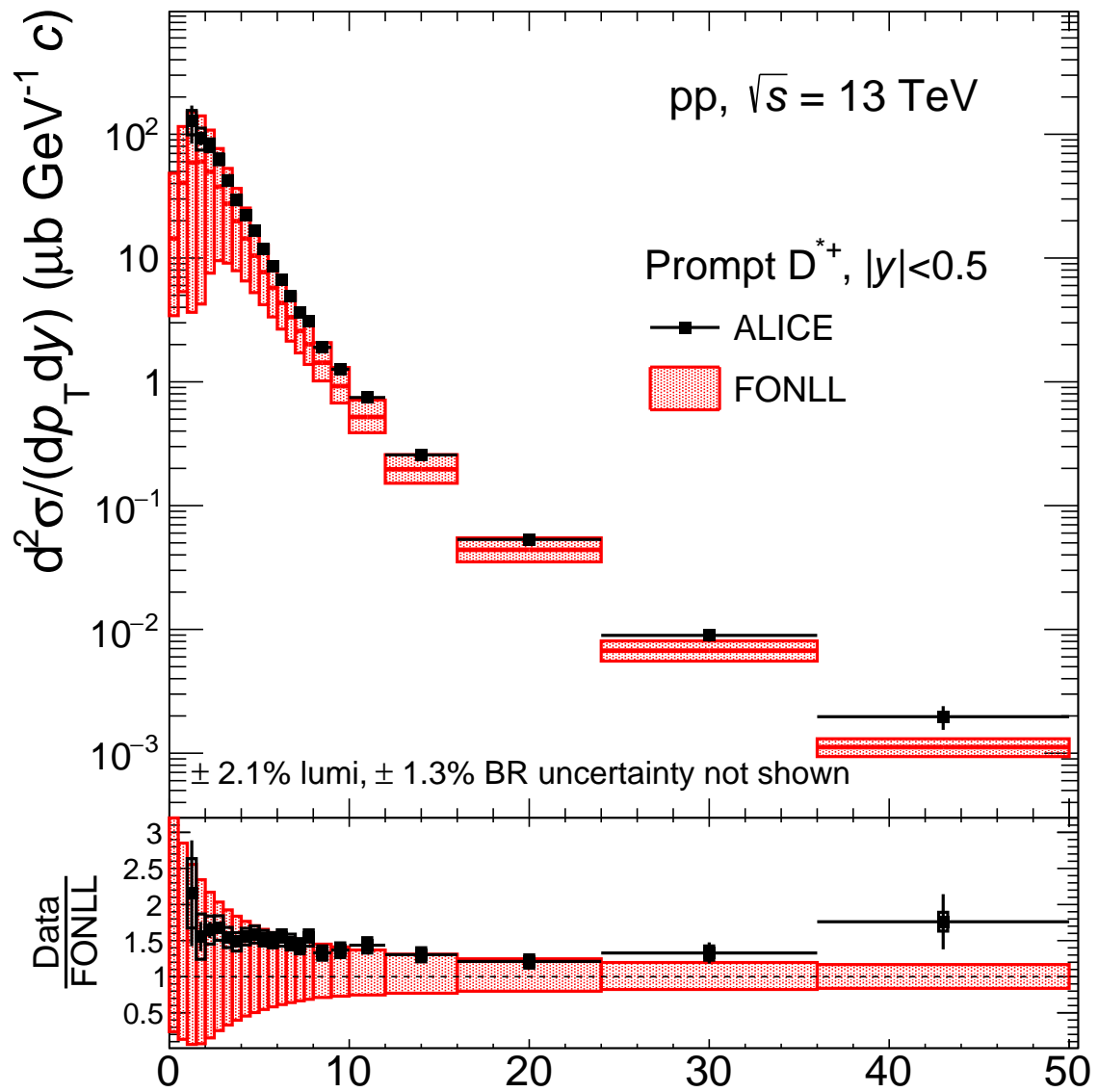


**Fig. 25:**  $p_T$ -differential inclusive production cross section of prompt D<sup>\*+</sup> mesons in pp collisions at  $\sqrt{s} = 13$  TeV compared with FONLL.

## References

- [1] ALICE Collaboration, J. Adam *et al.*, “Transverse momentum dependence of D-meson production in Pb-Pb collisions at  $\sqrt{s_{\text{NN}}} = 2.76$  TeV,” *JHEP* **03** (2016) 081, arXiv:1509.06888 [nucl-ex].
- [2] ALICE Collaboration, “Analysis note,” <https://alice-notes.web.cern.ch/node/576>.
- [3] T. Sjostrand, S. Mrenna, and P. Skands, “PYTHIA 6.4 Physics and Manual,” *JHEP* **05** (2006) 026, arXiv:hep-ph/0603175 [hep-ph].
- [4] P. Z. Skands, “The Perugia Tunes,” in *Proceedings, 1st International Workshop on Multiple Partonic Interactions at the LHC (MPI08): Perugia, Italy, October 27-31, 2008*, pp. 284–297. 2009. arXiv:0905.3418 [hep-ph].
- [5] X.-N. Wang and M. Gyulassy, “HIJING: A Monte Carlo model for multiple jet production in p p, p A and A A collisions,” *Phys. Rev.* **D44** (1991) 3501–3516.
- [6] ALICE Collaboration, S. Acharya *et al.*, “Measurement of  $D^0$ ,  $D^+$ ,  $D^{*+}$  and  $D_s^+$  production in pp collisions at  $\sqrt{s} = 5.02$  TeV with ALICE,” arXiv:1901.07979 [nucl-ex].